Effect of Thermal Conductivity, Reynolds Number, Aspect Ratio and Packing Arrangement on Radial Heat Transfer in Packed Beds

by

Nishith Kumar Reddy Gorla

nishith.gorla@mavs.uta.edu

Doctoral Dissertation Research

Presented to the Faculty of the Graduate School of
The University of Texas at Arlington in Partial Fulfillment
of the Requirements for the Degree of

DOCTOR OF PHILOSOPHY

Department of Mechanical and Aerospace Engineering
The University of Texas at Arlington
Arlington, TX 76019

August 2021

Doctoral Dissertation Committee

Dr Brian H. Dennis, Professor, MAE
Committee Chair

_ _

Dr Zhen Xue Han, Senior Lecturer, MAE
Committee Member

_ _

Dr Hyejin Moon, Associate Professor, MAE
Committee Member

_ _

Dr Kent Lawrence, Professor, MAE
Committee Member

_ _

Dr Chaoqun Liu, Professor, Mathematics
Committee Member

_ _

Abstract

The key motivation for this research is to study heat transfer developments in packed beds. The radial heat transfer enhancement of a packed bed in the laminar flow region is one of the major areas of ongoing research in mechanical, aerospace and chemical industries, especially the response of a packed bed during conjugate heat transfer with the fluid-solid interaction.

This computational study focuses on the impact of packing size, thermal conductivity, and arrangement on the radial heat transfer performance as a function of Reynolds number. A simple annular tube packed with circles (2D) and spheres (3D) is utilized for this study. The heat transfer performance is quantified by an Effective Thermal Conductivity (ETC), which indicates the overall effectiveness of the radial heat transfer performance. The studies focus on laminar flow since many applications using packed beds involve slow moving fluids to avoid large pressure drops.

Preliminary work focused on building an acceptable understanding of the problem in 2D before committing to time consuming 3D runs. A 2D rectangular packed bed is filled with different aspect ratios (tube to particle diameter ratio; $1 < \Lambda < 10$) and different porosity of circular particles to see how radial heat transfer is affected by these parameters. Two packing styles (regular & staggered) are designed to compare the effect of packing structure on ETC. Similarly, a 3D cylindrical packed bed is a packed bed filled with spherical particles of different aspect ratios ($2 < \Lambda < 10$), different heater temperatures and two packing structures (radial & hollow) to see how these parameters effect ETC.

Steady-state conjugate heat transfer analysis is performed for different values of parameters. The simulations are done for different packing materials in non-stagnant laminar

flow conditions ($Re_P < 10$) and the effects of Reynolds number and differing thermal conductivity of the materials on radial heat transfer is recorded. Periodic boundary conditions are imposed at the inlet and outlet.The simulations are run in COMSOL Multiphysics and, the Non-isothermal flow solver is used to couple the physics between the heat transfer and the fluid flow.

Results obtained show that radial thermal conductivity greatly relies on the particle size and packing arrangement in 2D packing. The staggered packing of aluminum circles with the aspect ratio(Λ) of 3.39 produces highest radial thermal conductivity while regular packing of aluminum circles with the aspect ratio of 3.21 produces highest radial thermal conductivity.The staggered packing of wood particles with the aspect ratio of 3.39 has the similar radial thermal conductivity of the regular packing of aluminum circles with the aspect ratio of 1.07.

In a 3D packed bed, ETC depends on heater temperature, thermal conductivity of a material, aspect ratio and packing arrangement. The ETC varies with thermal conductivity for different heater temperatures. The aspect ratio of 5.466 with radial packing of aluminum particles produces highest $\frac{K_e}{K_f}$ of 7.5. Whereas hollow packing of aluminum particles with aspect ratio of 2.733 producing highest $\frac{K_e}{K_f}$ of 6.5 for all heater temperatures.

The radial heat transfer remains constant by increasing the Reynolds number within the laminar flow region ($Re_P < 10$) for each aspect ratio, heater temperature, material and packing style.

Acknowledgement

Firstly, I would like to acknowledge my supervising professor, Dr.Brian H. Dennis for his exceptional guidance. His motivation and support in all aspects helped me to complete my doctoral degree. I would also like to acknowledge Dr.Zhen Xue Han, Dr.Hyejin Moon, Dr.Kent Lawrence, and Dr.Chaoqun Liu for serving in my thesis committee and for their valuable suggestions.

I would like to thank MAE department for financial support through out my studies at UTA. I would also like to acknowledge Sandeep Patil, Budhyant Venepalli, and Vivek Nair for their support and help in the process of my research.

Finally, I would love to express my deepest gratitude to my father, mother and brother for always being on my side in any kind of situation, giving constant emotional support and encouragement.

Contents

Nomenclature

Greek Symbols

Δ Change in

ϵ Void fraction

Λ Aspect ratio or Tube to particle diameter ratio

μ Dynamic viscosity of air, kg m^{-1}s^{-1}

Φ_S Shape factor or Sphericity factor

ρ Density of air, kg m^{-3}

θ Non dimensional temperature

Roman Symbols

C_D Drag coefficient

c_p Specific heat of air, KJ kg$^{-1}k^{-1}$

D Diameter

F Force vector, N s^{-1}

f Friction factor

f_D Drag force, N

g gravitational constant

h	Heat transfer coefficient, w m$^{-2}k^{-1}$
I	Lagrange multiplier
K	Thermal conductivity, w m$^{-1}k^{-1}$
L	Length of a bed, m
P	Pressure, pa
Q	Heat source, w m^{-2}
q_0	Heat flux vector, w m^{-2}
R	Radius of a packed bed, m
r	Radial direction
Re	Reynolds number
s	Surface area, m^2
T	Temperature, k
u	Velocity vector, m s^{-1}
V	Average velocity, m s^{-1}
v	Volume, m^3
V_0	Superficial velocity, m s^{-1}

Subscripts

avg	Average
b	Bulk
e	Effective
eff	Effective
f	Fluid

H Heater

P Particle

T Tube

$turb$ Turbulent

vd Viscous dissipation

W Wall

List of Figures

xiii

List of Tables

Chapter 1

Introduction

Packed bed reactors are utilized in many industrial applications including chemical, manufacturing and separation/filtration. They are found in different types of heat transfer applications like drying, heat exchangers, and solar thermal storage. A packed bed is typically a vertical tube filled with a packing material. The packing material can be made of steel, aluminum or, glass and are shaped as spheres, cylinders, hollow cylinders, irregular particles, or Raschig rings. As packed beds have a wide range of applications in heat and mass transfer, there are many parameters to consider in their design.

The heat transfer performance is quantified by an Effective Thermal Conductivity (ETC), which indicates the overall effectiveness of the radial heat transfer performance. The packed bed's ETC function of wall heat transfer coefficient, wall temperature, extrapolated wall temperature and radial temperature. These parameters extracts from the COMSOL and calculate ETC of a bed.

1.1 Thermal Energy Storage and Applications

Gianpkoplis, Warren, and et.al [1,2] emphasize that there is a wide range of energy storage techniques available for different types of electrical applications. The packed bed reactor does not have any geographical constraints and limitations. This type of energy storage is economically low, helps to control diminishing fossil fuels and most importantly is atmospherically friendly when compared to other renewable energy storages. Packed

bed thermal storage has many heating applications such as solar power storage, advanced adiabatic compressed air energy storage, pumped thermal energy storage, and liquid air energy storage. The performance of thermal energy storage depends on many parameters such as heat transfer between the solid and fluid, thermal conduction of packed bed and energy loss from the wall. Moreover, thermal storage application changes according to the axial flow and radial flow of fluid.

1.2   Packing Structure

The pressure loss and heat transfer efficiency depend on the packing structure of a packed bed. There are mainly two types of packing structures available. One is structured packing and the other is random packing. The structured packing beds have different forms, including simple cubic, face centered cubic and body centered cubic. The randomly packed structure does not come under structured packing and are more convenient to construct. In this research, packing arrangement is considered that the packing is structured and uniform everywhere. The structured packing beds produce less pressure drop and high thermal efficiency, whereas randomly packed structures produce high pressure drop and poor lateral heat transport since it has improper voids everywhere in the bed[23]. So, structured packing maintains homogeneous fluid flow and enhancement of radial heat transfer in packed beds which is important for this thesis.

1.3   Research Objectives

This research is a numerical study that aims to provide an understanding of the effect of aspect ratio, thermal conductivity of a packed material, heater temperature, and Reynolds number on radial heat transfer within the laminar flow region ($Re_P < 10$). The aspect ratios of a packed bed 1< Λ <10, different types of packing material(brick, iron, steel, and aluminum), different heater temperatures(400 K, 500 K, and 600 K), and different types of packing arrangement (radial & hollow) is recorded to see how these parameters affect radial heat transfer in non-stagnant laminar flow conditions.

Chapter 2

Literature Survey

The effect of radial heat transfer in a packed bed mainly depends on the bed to particle diameter ratio, particle material properties and shape of the particle. Demirel et.al [3] have emphasized that the ratio of effective radial thermal conductivity and fluid thermal conductivity ($\frac{K_e}{K_f}$)as a function of Reynolds number for different materials. Dixon [4] ceramic hollow cylinders of aspect ratio (Λ) of 5.1 producing highest $\frac{K_e}{K_f}$ of range is about 25-120 for the Reynolds numbers range is about 300-1200. In this case, $\frac{K_e}{K_f}$ linearly increases with the Reynolds number.

Demirel's [3] polyvinyl chloride Raschig rings particles of $5.6 < \Lambda < 6.6$, Dixon's [4] steel spheres aspect ratio of 7.9, and Freiwald and Paterson's [5] ceramic spheres of aspect ratio of 7.7 producing $\frac{K_e}{K_f}$ of range is about 20-80 and for the Reynolds numbers range is about 300- 1400. Smirno et.al [6] explains in their research that the expanded polystyrene spheres of $4.5 < \Lambda < 7.5$, and Dixon [4] spheres of aspect ratio of 6.4 producing least $\frac{K_e}{K_f}$ of range is about 10-60 and for the Reynolds numbers range is about 300-1400. So, $\frac{K_e}{K_f}$ is increasing with the Reynolds number. However, it is not linear.

Zehua et.al [7] emphasizes pressure drop as one of the important things to consider in packed beds. Hollow structured packed bed (HPSB) of spheres produce less pressure drop and better heat transfer efficiency. As aspect ratio increases in HPSB, pressure drop increases and heat transfer coefficient decreases. The aspect ratio of 2.88 produces the highest overall heat transfer coefficient and HPSB reduces about 80 pressure drop when compared to random packing. Smirno et.al [6] conducted an experiment on use of shaped

particles such as ceramic cylinders, ceramic rings and ceramic wheels in a packed bed which enhance radial heat transfer and reduces pressure drop.The radial thermal conductivity increases as channel cross section increases. So, packing arrangement and apect ratio are important parameters in designing a packed bed.

The aspect ratio varies depending upon the industrial applications. Peng, Borkink, and et.al summarizes in their research that the radial effective thermal conductivity doesn't only depend on particle diameter, but also depends on the aspect ratio. Dixon [4] also explained that for a small aspect ratios $1 < \Lambda < 2$, strong wall effects are taken place which produce good effective thermal conductivity and Nusselt number. This performance is even applicable for aspect ratio less than 4.

Peng et.al [8] summarizes a packed bed with small aspect ratio, the fluid to wall heat transfer coefficient periodically oscillating and producing maximum at inlet of the duct. The heat transfer coefficient increases as Reynolds increases for the same aspect ratio. Ying et.al [10] emphasizes that the small aspect ratio of ring type packing produces more effective radial heat transfer than sphere packing, and which are used in industries often. Under the equivalent Reynolds number interstices, the fluid to wall heat transfer coefficient decreases as aspect ratio increases. However, Borkink and Westerterp [9] said that the smaller aspect ratios of glass sphere particles and alumina ring type particles producing same wall to fluid heat transfer coefficient. According to Ying[10] the particle arrangement places crucial role on radial heat transfer performance of packed bed.

Mariana et.al [11] summarizes that $5 < \Lambda < 15$ of sphere particles produces higher radial effective thermal conductivity in many industrial applications. Borkink, Dong-Young et.al [9,12] emphasize that the heat transfer parameters depend on height of the packed bed and Nusselt number decreases when height of the bed increases.

Yusuke et.al [13] emphasizes void fraction and contact between the particles are more important parameters to consider improving Effective Thermal Conductivity (ETC) in a packed bed reactor. The thermal convection can't be neglected at lower Biot number and combination of thermal conduction, convection and radiation helps to calculate more accurate temperature in packed bed reactors. Mandal et.al explained that the [14] ETC

4

is rapidly increasing with the surficial velocity and particle size.Mandal et.al also explain that helium is more inert than air as a working fluid medium which helps to enhance the ETC.

Chapter 3

Approach and Methodology

3.1 Governing Equations for a Packed Bed

The governing equations for packed beds which are used to describe mass, momentum and energy balances in packed beds. There are some assumptions made in order to reduce the complication.

- Steady state heat transfer.
- In-compressible flow.
- Porosity doesn't depend on time and the position.
- Voids spaces are interconnected.
- The fluid particles in voids spaces are in single phase.
- The packed particles are stagnated with respect to fluid.

There are many mathematical models to express the fluid flow behavior, but most of the partial differential equations are used to obtain accurate and complete results.

As well known that density is neglected in incompressible flows because there won't be a significant variation in liquids and gases with moderate pressure and temperature. The viscous dissipation term is neglected in laminar flow region.

3.1.1 Conservation of Mass

$$\rho \nabla \cdot (\vec{u}) = 0 \tag{3.1}$$

The above equation represents conservation of mass in a packed bed with porous media which is also called continuity equation. The equation (3.1) states that rate of change of fluid mass within the packed bed equal to mass flux entering the control volume.

3.1.2 Conservation of Momentum

$$\rho(\vec{u} \cdot \nabla)(\vec{u}) = \nabla \cdot [-P[I] + [A]] + \vec{F} + \rho \vec{g} \tag{3.2}$$

Where,

$$A = \mu(\nabla \vec{u} + (\nabla \vec{u})^T)$$

The momentum equation explains the physical significance behind the viscous forces (A) which is included in equation (3.2). The pressure loss caused the flow between inlet and outlet of a bed. The body force vector and gravitational force vector are other important parameters to create momentum.

The Darcy's law applicable for fluid flow through a porous media and which is only applicable for packed beds with Reynolds number less than 10. Other effects, such as resistance due to turbulence must consider for higher Reynolds numbers.

3.1.3 Conservation of Energy

$$(\rho c_p)\vec{u} \cdot \nabla T + \nabla \cdot \vec{q} = Q + q_0 + Q_{vd} \tag{3.3}$$

Where,

$$\vec{q} = -K \cdot \nabla T$$

$$\rho c_p = Volumetric\ heat\ flux, \frac{Jm^3}{k}$$

$$Q_{vd} = \tau : \nabla \vec{u} + Q_{turb}$$

The Navier-Stokes equations provide solution for pressure and velocity field. The energy equation must be included when temperature data is desirable.

The packed bed in this research deals with heat transfer in both fluids and solids. The heat transfer equations don't change with flow type which means heat transfer physics

7

would be the same for both laminar flow and turbulent flow conditions. Viscous dissipation is neglected for laminar flows since it doesn't create any heat flow.

3.2 Drag Coefficient and Types of Drag in a Packed Bed

[1], [2]emphasize that it is very important to predict frictional losses and forces on the submerged objects in a bed of solids. The transfer of momentum perpendicular to the surface resulted in tangential shear stress/drag on the smooth surface parallel to direct of flow and the force exerted by the fluid on a solid in the direction of flow in a bed is called wall/skin drag. The skin friction drag exists for any surface contact with fluid, in addition if any flow is not flowing parallel to the surface (spheres presence in a bed leads to this kind of flow) which is called form drag.

The flow over a flat plate results just the skin friction/ tangential stress, but in case of flow over a sphere in a packed bed produces the skin friction drag due to velocity gradient in the boundary layer and the form drag due to the sphere outside boundary layer flow changes its direction. The form drag intensity depends upon the particle shape and Reynolds number. The flow drag can be reduced by streamline the body design.

Laminar region for low Reynolds number Re_P <10 experimental drag force of a sphere is same as theoretical stokes law equation.

$$F_D = 3\pi\mu D_P V_0 \tag{3.4}$$

Drag coefficient of sphere (C_D) is 0.44 for Reynolds number range of $1000 < Re < 2\text{x}10^5$. Boundary layer separation, turbulent flow and separation point shift occurs at Reynolds number Re=$3\text{x}10^5$.

The resistance of the flow of a fluid through voids in a bed of solids is called total drag of all particles in a bed. As in the drag of a single particle doesn't create sharp transition between laminar and turbulent flow as like that occur in a flow through pipes or channel of constant cross section.

3.3   Pressure Drop Calculation for a Packed Bed

[1] and [2] emphasize that the most common method of calculating the pressure drop through a bed solid are based on the estimate of drag on a solid boundary of the tortuous channels through a bed. Actual channels are irregular in shape, have variable cross sections, have different orientations, and are highly interconnected. So, dividing the packed bed into n number of capillaries and determine the void fraction.

Total surface to volume ratio, void fraction, particle diameter, density of a fluid, viscosity of a fluid, and length of the packed bed are the most essential parameters to determine the pressure drop in a packed bed.

3.3.1   Shape Factor

Total surface area (s_P) = number of particles * surface area of a particle.
Total volume (v_P) = number of particles * volume of a particle.

$$\frac{s_P}{v_p} = \frac{6}{\Phi_S D_P} \tag{3.5}$$

Where Φ_S is Sphericity factor. For sphere Φ_S=1 and for irregular particles,

$$\Phi_S = \frac{\frac{s_P}{v_P}\,Sphere}{\frac{s_P}{v_P}\,Particles} \tag{3.6}$$

In general, Φ_S=0.874 for cylinder $D_P = L$, Φ_S=0.3 for Raschig rings.

The flow entering the packed bed is superficial velocity or empty tower velocity which is denoted with V_0 and the average velocity in the channel is

$$V = \frac{V_0}{\epsilon} \tag{3.7}$$

9

3.3.2 Ergun Equation for Pressure Drop

The pressure drop is calculated using Ergun's equation in a packed bed as follows:

$$\frac{\Delta P}{L} = \frac{150 V_0 \mu}{\Phi_s^2 D_P^2} \left[\frac{1 - \epsilon^2}{\epsilon^3} \right] + \frac{1.75 \rho V_0^2}{\Phi_s D_P} \left[\frac{1 - \epsilon}{\epsilon^3} \right] \qquad (3.8)$$

The volume fraction of a packed bed is (1- ϵ), where ϵ is porosity or void fraction of a bed. If the particles are porous, pores are generally too small to permit any significant flow through them. The external porosity within a bed is much higher than porous particles in a bed.

The pressure drop equation applies for both laminar and turbulent cases. The first of an equation represents the viscous losses and second part represents kinetic energy losses in a packed bed.

$$\frac{\Delta P}{\frac{3\mu V_0}{D_P \epsilon}} = \frac{50 L}{\Phi_S D_P^2} \left[\frac{1 - \epsilon^2}{\epsilon^2} \right] \qquad (3.9)$$

The equation (3.9) represents pressure drop corresponding to friction head. It applicable to small Reynolds numbers which is $Re_P < 10$.

$$\frac{\Delta P}{\frac{\rho V_0^2}{2\epsilon^2}} = 2 * 1.75 \frac{L}{\Phi_s D_P} \left[\frac{1 - \epsilon}{\epsilon} \right] \qquad (3.10)$$

The equation (3.10) represents pressure drop corresponding to the velocity head. For porosity value $\epsilon = 0.4$, the equation would be

$$\frac{\Delta P}{\frac{\rho V_0^2}{2\epsilon^2}} = 5.25 \frac{L}{\Phi_s D_P} \qquad (3.11)$$

The equation (3.11) tells that the pressure drop corresponding to a loss of 5.25 velocity head for each layer of particles in a packed bed. It applicable to Reynolds number $Re_P > 1000$.

The non dimensional pressure drop equation for a spherical packing particles is

$$\frac{\Delta P}{L} = \frac{\rho V_0^2 (1 - \epsilon)}{D_P \epsilon^3} \left[\frac{150}{Re_P} + 1.75 \right] \qquad (3.12)$$

10

3.4   Reynolds Number Calculation for a Packed Bed

The general Reynolds number formula for a spherical particle is

$$Re = \frac{\rho V D_P}{\mu} \tag{3.13}$$

For a packed bed, replace particle diameter with equivalent diameter of a channel and replace superficial velocity with average velocity in the channel.

Hence, Reynolds number for a packed bed is

$$Re_p = \frac{2}{3} \frac{\rho V_0 D_P}{\mu(1-\epsilon)} \Phi_S \tag{3.14}$$

Reynolds number for a packed bed of spherical particles is

$$Re_p = \frac{\rho V_0 D_P}{\mu(1-\epsilon)} \tag{3.15}$$

From many experimental results, laminar flow for a packed bed is $Re_P < 5 - 10$ and turbulent flow for a packed bed is $Re_P > 1000$.

3.5   Friction Factor Calculation for a Packed Bed

[1]In general friction factor for Newtonian fluid flow through a single column is

$$f = \frac{1}{\rho V^2} [\frac{\Delta P}{L} \frac{D}{2}] \tag{3.16}$$

The friction factor for packed bed would be

$$f_p = [\frac{-\Delta P}{L}][\frac{D_p}{\rho V_0^2}][\frac{\epsilon^3}{1-\epsilon}] \tag{3.17}$$

The friction factor for spherical particles would be

$$f_p = [\frac{150}{Re_P} + 1.75] \tag{3.18}$$

The $\frac{150}{Re_P}$ represents viscous losses in a bed and [1.75] represents kinetic losses in a packed bed. The friction factor decreases as Reynolds number increases. It is clearly showing that, there would not be much viscous losses in a turbulent flow and friction factor stays constant.

3.6 Effective Thermal Conductivity Calculation for a 2D Packed Bed

The effective thermal conductivity for a 2D packed bed is calculated using the following equation:

$$Q = -\frac{K_e \Delta T_{avg}}{L} \qquad (3.19)$$

Where; Q = Heat flux ($\frac{W}{m^2}$), K_e = Effective Thermal Conductivity ($\frac{W}{m-k}$), L= Distance between the two walls (m), $\Delta T_{avg} = T_{avg1}$ - T_{avg2} (k)
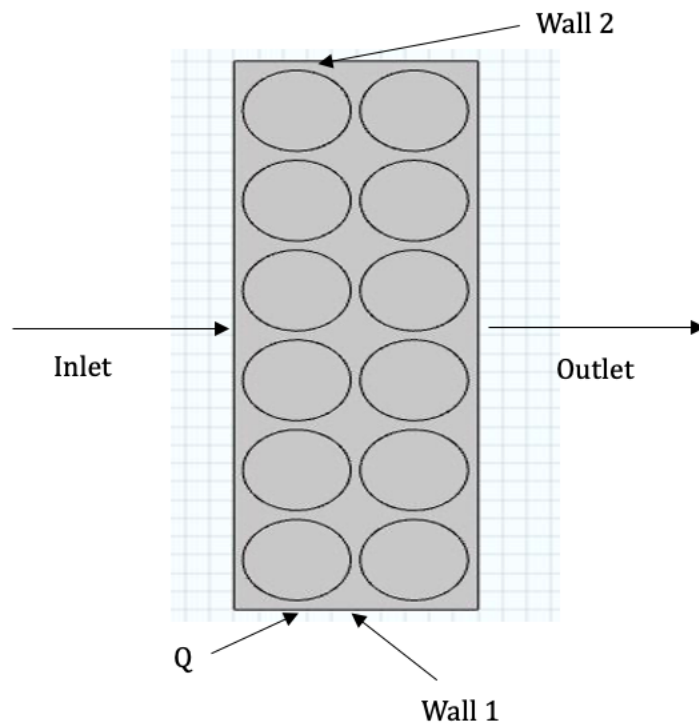
Figure 3.1: 2D packed bed geometry

A 2D packed bed is filled with circular packing particles. The left wall act as a inlet, right wall act as a outlet. The lower wall subjected to heat flux and upper wall subjected to natural convection as shown in Figure 3.1.

The effective thermal conductivity depends on the heat flux, length of a packed bed and difference between the walls temperatures.

3.7 Effective Thermal Conductivity Calculation for a 3D Packed Bed

The effective thermal conductivity for a 3D packed bed is calculated using the following equation:

$$-K_{eff}\frac{\partial T}{\partial r} = h_w(T_w - T_b) \tag{3.20}$$

The temperature distribution is defined by the polynomial equation

$$T = a_0 + a_1 r + a_2 r^2 + a_3 r^3 \tag{3.21}$$

Boundary conditions for cylindrical packed bed of spheres are

$$r = 0, T = T_H$$

$$r = R, T = T_W$$

$$r = 0, \frac{\partial T}{\partial r} = 0$$

The final equation for effective thermal conductivity is

$$K_{eff} = \frac{h_w(T_w - T_b)}{T_w - T_H}R \tag{3.22}$$
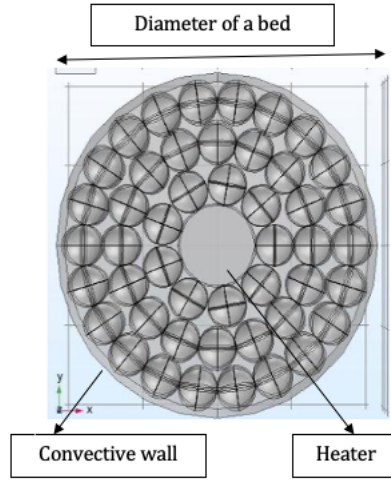
Figure 3.2: 3D packed bed geometry

A 3D packed bed is filled with spherical packing particles. The cylindrical heater is placed in the middle of a bed. The packed bed wall subjected to natural convection as shown in Figure 3.2.

The effective thermal conductivity depends on the heater temperature, diameter of a bed, heat transfer coefficient of a bed wall, and bulk temperature. The bulk temperature of a packed bed is calculated using following equation:

$$T_b = \frac{\int_0^R T \, dr}{\int_0^R dr} = a_0 + \frac{a_1}{2}r + \frac{a_2}{3}r^2 + \frac{a_3}{4}r^3 \tag{3.23}$$

14

3.8 Different Methods to Obtain the Effective Thermal Conductivity and Predict Temperature of Heat Generating Body

Previous researcher implemented CVSAM for obtaining effective thermal conductivity and its sensitivity. This calculated sensitivity can be advantageous in determining reliability of the system for example ball grid array package , moreover neural network can be used to predict temperature of heat generating body [25,26,27,28,29].

Finite volume code has been developed for capturing heat transfer phenomena in heat generating bodies. Furthermore sensitivity is derived using CVSAM, which is helpful for predicting reliability of system as ball grid array package. in addition, neural network can be used to predict temperature of heat generating body [25,26,27,28,29].

Complex Variable Semi Analytical method (CVSAM) is advantageous in capturing sensitivity regardless of determining step size, which has been implemented in inverse analysis. These sensitivity values are helpful in measuring reliability of the system including ball grid array package. moreover, machine learning is used to predict temperature of heat generating body [25,26,27,28,29].

Numerical inverse analysis is used to predict properties of heat generating material by measuring temperature at outer boundary. Accuracy and efficiency of the method is enhanced by using accurate sensitivity information by use of Semi-Analytical Complex Variable Method (CVSAM). Sensitivity information is beneficial in determining reliability of the system like ball grid array package. In addition, machine learning can be used to predict temperature of heat generating bodies [25,26,27,28,29].

3.9 Computational Validation with Experimental Analysis of Low Reynolds Number Flow Around a Heated Cylinder

This section presents the validation between experimental and computational results of different cylinder temperatures within the laminar flow region. The Experiments were carried out in a wind tunnel with open test section [16]. The cylinder was placed horizontally normal to its axis and cylinder powered electrically. The flow around cylinder was measured by creating the vertical plane normal to the axis of a cylinder.

A circle is placed in the center of a 2D rectangular duct which is designed in COMSOL. The top and bottom walls are considered as symmetric. The cylinder surface temperature operates at five different temperatures (297, 373, 473, 573, 673 K). The measurements were carried out for three velocities (0.3, 0.45, 0.6 $\frac{m}{s}$) and each velocity is operated at all five temperatures. The conjugate heat transfer model is used, and non-isothermal Multiphysics is used in order to couple the fluid and the solid.
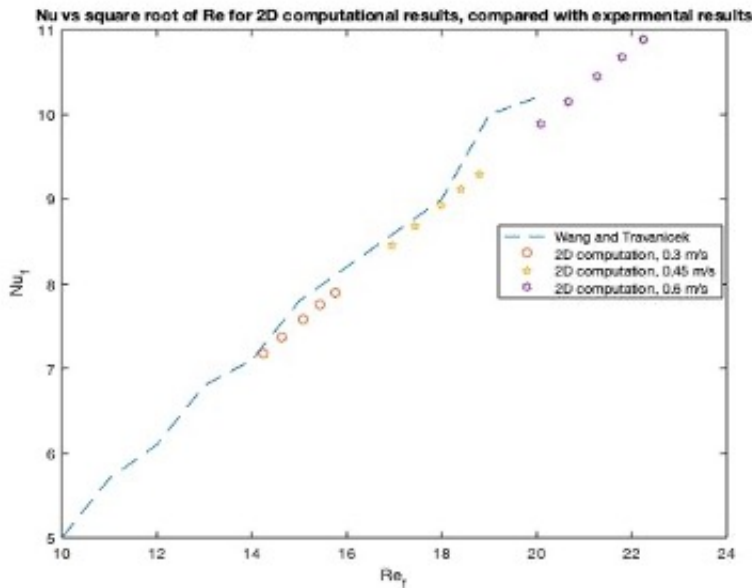
Figure 3.3: Analysis of low Reynolds number flow over heated cylinder

16

Figure 3.3 shows the variation of Nu_f as a function of $Re_{Rep}^{0.5}$ (Re_f) and 2D computational results are good agreement with the Wang and Travanicek 's [17] experimental results.

Chapter 4

Thermally Fully Developed Flow for Two Parallel Plates

This chapter is to understand fully developed flow is attain when two plates are operating at same temperatures and inlet temperature is different. The temperature profile is no longer change after certain length.

4.1 Flow through Two Parallel Plates when the Velocity Profile is Fully Developed and Temperature Profile is Developing

4.1.1 Analytical Solution for Two Parallel Plates
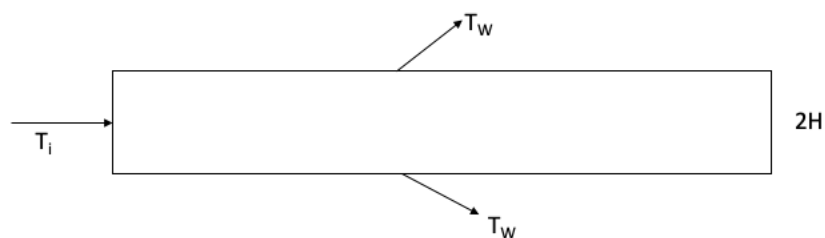
Figure 4.1: Two parallel plates

Two parallel plates separated by a distance of 2H, which both walls are subjected to temperature of T_W, and inlet wall is at temperature of T_i as shown in Figure 4.1.

[19],[20],& [21] Some assumptions are made to reduce the complicity of an energy equation which steady state heat transfer, axial thermal conduction is neglected, and velocity profile is fully developed.The energy equation would be following:

$$\rho c_p u \frac{\partial T}{\partial x} = k \frac{\partial^2 T}{\partial y^2} \tag{4.1}$$

Converting into non-dimensional form of energy equation by introducing non dimensional parameters

$$\bar{y} = \frac{y}{H}, \bar{x} = \frac{x/H}{RePe}, Pe = \frac{\rho c_p H U}{k}$$

Fully developed velocity profile is

$$U(\bar{y}) = \frac{3}{2}[1 - \bar{y}^2] = \frac{u(y)}{U_{avg}} \tag{4.2}$$

$$\theta(\bar{x}, \bar{y}) = \frac{T_b - T_W}{T_i - T_W} \tag{4.3}$$

Where T_i is inlet temperature, T_b is bulk temperature, and T_W is wall temperature. The non dimensional energy equation would be:

$$\frac{u}{U} \frac{\partial \theta}{\partial \bar{x}} = \frac{\partial^2 \theta}{\partial \bar{y}^2} \tag{4.4}$$

Method of separation of variables

$$\theta(\bar{x}, \bar{y}) = X(\bar{x})Y(\bar{y})$$

$$\frac{u}{U} \frac{X^1}{X} = \frac{Y^{11}}{Y}$$

$$\frac{X^1}{X} = (\frac{u}{U})^{-1} \frac{Y^{11}}{Y} = -\lambda^2$$

The equations would be:

$$X^1(\bar{x}) + \lambda^2 X(\bar{x}) = 0$$

19

$$Y^{11}(\bar{y}) + \lambda^2(\frac{u}{U})Y(\bar{y}) = 0$$

Boundary conditions are

$$\bar{x} = 0, \theta = 1$$

$$\bar{y} = 0, \frac{\partial \theta}{\partial y} = 0$$

$$\bar{y} = 1, \theta = 0$$

The temperature distribution would be:

$$\theta(\bar{x}, \bar{y}) = \sum_{n=0}^{\infty} C_n Y_n e^{-\lambda^2 \bar{x}} \tag{4.5}$$

Apply B.C, $\bar{x} = 0, \theta = 1$

$$1 = \sum_{n=0}^{\infty} C_n Y_n$$

Integrate both sides by $Y_m(\frac{u}{U})d\bar{y}$

$$\int_0^1 (\frac{u}{U}) Y_m d\bar{y} = \int_0^1 \sum_{n=0}^{\infty} (\frac{u}{U}) C_n Y_m Y_n d\bar{y}$$

Using the orthogonality condition from Sturm Liouville equation

$$\int_0^1 (\frac{u}{U}) Y_m Y_n d\bar{y} = 0, \; if \; n \neq m$$

$$\int_0^1 (\frac{u}{U}) Y_m Y_n d\bar{y} = N_n, \; if \; n = m$$

So,

$$\int_0^1 (\frac{u}{U}) Y_n d\bar{y} = C_n \int_0^1 (\frac{u}{U}) Y_n^2 d\bar{y}$$

$$C_n = \frac{\int_0^1 (\frac{u}{U}) Y_n d\bar{y}}{\int_0^1 (\frac{u}{U}) Y_n^2 d\bar{y}} \tag{4.6}$$

Let us integrate second order ODE Y_n

20

$$\frac{d^2\theta}{d\bar{y}^2} = -\lambda^2\left(\frac{u}{U}\right)\bar{Y}_n$$

$$\int_0^1 \frac{d^2\theta}{d\bar{y}^2} = -\int_0^1 \lambda^2\left(\frac{u}{U}\right)\bar{Y}_n d\bar{y}$$

$$\int_0^1 \lambda^2\left(\frac{u}{U}\right)\bar{Y}_n d\bar{y} = -[\bar{y}\frac{dY_n}{d\bar{y}}]_{\bar{y}=1} + [\bar{y}\frac{dY_n}{d\bar{y}}]_{\bar{y}=0}$$

As known that $[\frac{dY_n}{d\bar{y}}]_{\bar{y}=0} = 0$, Then above equation becomes

$$\int_0^1 \lambda^2\left(\frac{u}{U}\right)Y_n d\bar{y} = -[\bar{y}\frac{dY_n}{d\bar{y}}]_{\bar{y}=1}$$

$$\int_0^1 \left(\frac{u}{U}\right)Y_n d\bar{y} = -\frac{1}{\lambda_n^2}[\frac{dY_n}{d\bar{y}}]_{\bar{y}=1}$$

$$C_n = \frac{-\frac{1}{\lambda_n^2}[\frac{dY_n}{d\bar{y}}]_{\bar{y}=1}}{\int_0^1 \left(\frac{u}{U}\right)Y_n^2 d\bar{y}}$$

$$\int_0^1 \left(\frac{u}{U}\right)Y_n^2 d\bar{y} = \frac{1}{2\lambda_n}\left(\frac{\partial Y_n}{\partial \lambda_n}\frac{dy_n}{d\bar{y}}\right)_{\bar{y}=1}$$

$$C_n = \frac{-\frac{1}{\lambda_n^2}[\frac{dY_n}{d\bar{y}}]_{\bar{y}=1}}{\frac{1}{2\lambda_n}\left(\frac{\partial Y_n}{\partial \lambda_n}\frac{dy_n}{d\bar{y}}\right)_{\bar{y}=1}}$$

By simplifying it, we get

$$C_n = -\frac{2}{\lambda_n}\frac{1}{\left(\frac{\partial Y_n}{\partial \lambda_n}\right)_{\bar{y}=1}}$$

The Y_n is find from the recursive relation.

$$Y_n = \sum_0^\infty B_n(\bar{y})^n$$

$B_0 = 1, B_2 = -\frac{3}{4}, B_1 = B_3 = B_5.. = 0$ since temperature is symmetric about x axis.

$$B_n = \frac{3}{2}\left[\frac{B_{n-4}}{\lambda_n^2} - B_{n-2}\right]\frac{1}{n(n-1)}, \quad for \ n = 4, 6, ...$$

Table 4.1: Axial length and Temperature distribution[20]

$\frac{x/D_H}{Re_D Pr}$	θ_b
0.00001	0.996584
0.000015	0.995526
0.00002	0.994584
0.00003	0.992909
0.00004	0.991416
0.00006	0.988764
0.00008	0.9864
0.0001	0.984231
0.0002	0.975038
0.0008	0.937615
0.001	0.927736
0.002	0.886037
0.0002	0.975038
0.01	0.675032
0.02	0.498044
0.03	0.36832
0.04	0.272413
0.1	0.0445919
0.2	0.00218425
0.3	0.000106991
0.4	$5.24075 * 10^{-6}$
0.6	$1.25744 * 10^{-8}$

The final temperature distribution is

$$\theta(\bar{x}, \bar{y}) = -2 \sum_0^\infty \frac{Y_n e^{(-\lambda^2 \bar{x})}}{\lambda_n (\frac{\partial Y_n}{\partial \lambda_n})_{\bar{y}=1}}$$

The Eigen values and Bulk temperature are obtained using Mathematica program

Table 4.2: Eigen Values[20]

λ_n	C_n
1.6816	0.6002
5.6696	-0.1503
9.6682	0.08041
13.6677	-0.05161
17.6674	0.03982
$4n + \frac{5}{3}$	$(-1)^n 1.356\lambda^n$

4.1.2   Computational Solution for Two Parallel Plates

Figure 4.2: Geometry of two parallel plates

The geometry of a two parallel plates shown in Figure 4.2, where inlet is at temperature of 300 K and both walls are operating at 400 K.

Figure 4.3: Velocity contour and profile of two parallel plates

The fully developed velocity contour shown in Figure 4.3 and the velocity profile is taken from the equation (4.2). The velocity is constant throughout the duct.

Initially, temperature profile is not fully developed since inlet temperature is operating at different temperature. Within a small distance flow becomes thermally fully developed

Figure 4.4: Temperature contour and profile of two parallel plates

as shown in Figure 4.4.

This is an evidence that flow becomes thermally fully developed instantly if operating with same wall temperatures.
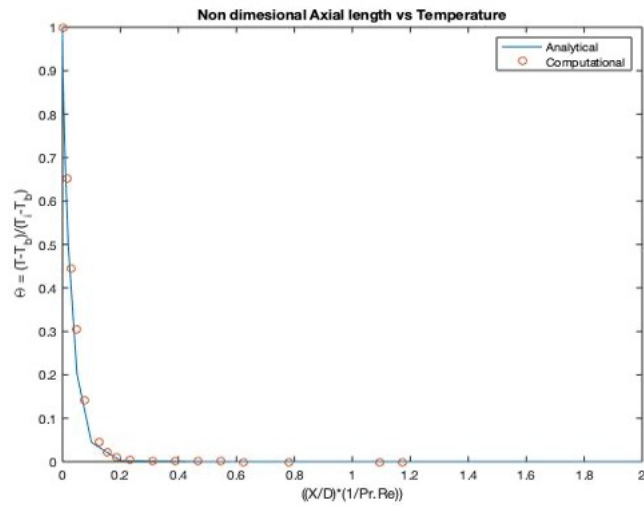
Figure 4.5: Non dimensional axial length vs temperature for two parallel plates

The Figure 4.5 showing that both analytical and computational solutions are matching and also following the same trend.It also shows that the non dimensional axial length, $\bar{x} = \frac{x/H}{Re.Pe} > 0.2$ flow becomes fully developed as shown in Table 4.1.

4.1.3 Computational Solution for Two Parallel Plates with Different Temperatures
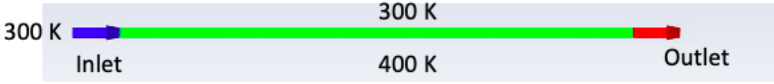
Figure 4.6: Geometry of two parallel plates

The geometry of a two parallel plates shown in Figure 4.6, where inlet and upper wall has same temperature of 300 K and lower wall is operating at 400 K.
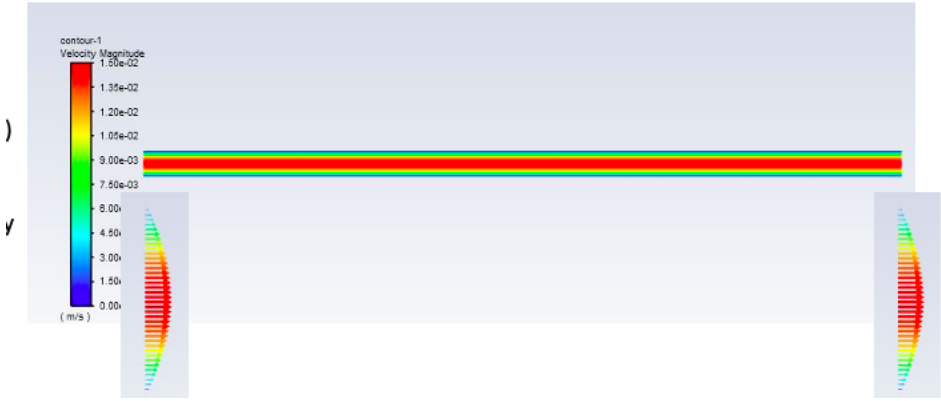
Figure 4.7: Velocity contour and profile of two parallel plates

The fully developed velocity contour shown in Figure 4.7 and the velocity profile is taken from the equation (4.2). The velocity is constant throughout the duct.

Initially, temperature profile is not fully developed since both plates are operating at different temperatures. It continues the same trend for small distance and then after flow becomes thermally fully developed as shown in Figure 4.8.

This is a computational evidence that flow becomes thermally fully developed if operating at two different wall temperatures.

Initially, the inlet wall is at 300 K and by moving in axial direction, the flow becomes fully developed after 15 mm in parallel plates shown in Figure 4.9.
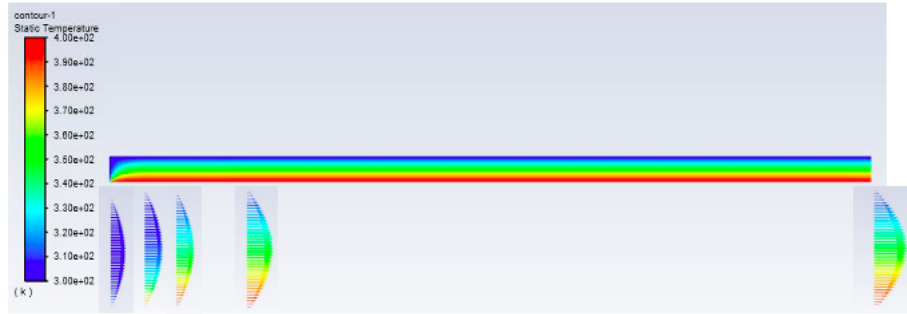
Figure 4.8: Temperature contour and profile of two parallel plates
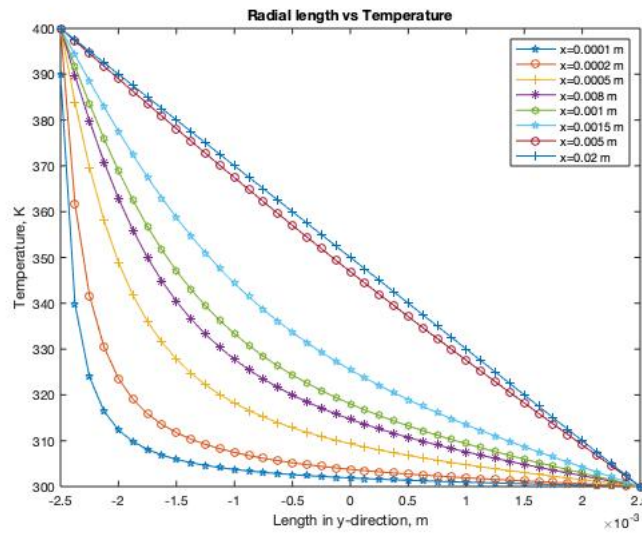
Figure 4.9: Radial length vs temperature for two parallel plates computationally

Chapter 5

Design and Analysis

5.1 Flow Chart for a Computational Model

The computational models of a packed bed are developed in COMSOL multi-physics. There are some steps to setup a computational model shown in Figure 5.1, such as design a geometry, make material selections, select heat transfer and fluid flow physics, do the mesh, perform a study and finally get results.

These obtained results are help to do the data analysis by providing mass weighted average wall temperature, velocity magnitude, and bulk temperature of a packed bed. The non-isothermal temperature contours and velocity contours are also captured for better understanding.

The parametric sweep, such as different Reynolds numbers and different heater temperatures and also material sweep are used in a study to get all required results at a same time.
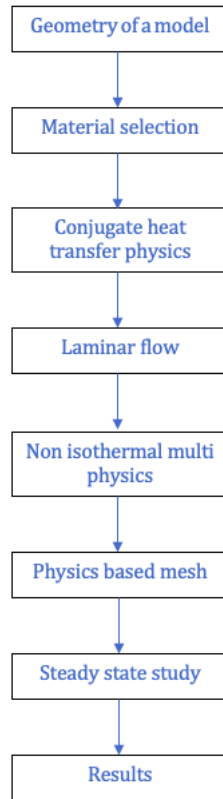
Figure 5.1: Schematic diagram for a computational model

5.2 General Design Constraints and Design of a Packed Bed

In general, the diameter of a packed bed to diameter of a particle should have minimum of 8:1 to 10:1. However, this requirement might change according to the application. The positioning of packed bed reactors for most of the applications should be vertical for a proper channeling and to avoid more void age on one end.

5.2.1 2D Packed Bed Design

The 2D rectangular packed bed is assumed to be length of 60 mm and width of 20 mm for current research. The bed is filled with the solid circular particles as shown in

Figure 5.2 at different aspect ratios $(1 < \Lambda < 10)$. The models are designed and simulated in COMSOL Multiphysics. The solid circular particles are considered to be made up of aluminum, brick and other material type to compare the effect of thermal conductivity on radial heat transfer. In the Figure 3.9, geometry of different aspect ratio with same porosity is shown. There is a space between the circles in order to pass the flow.
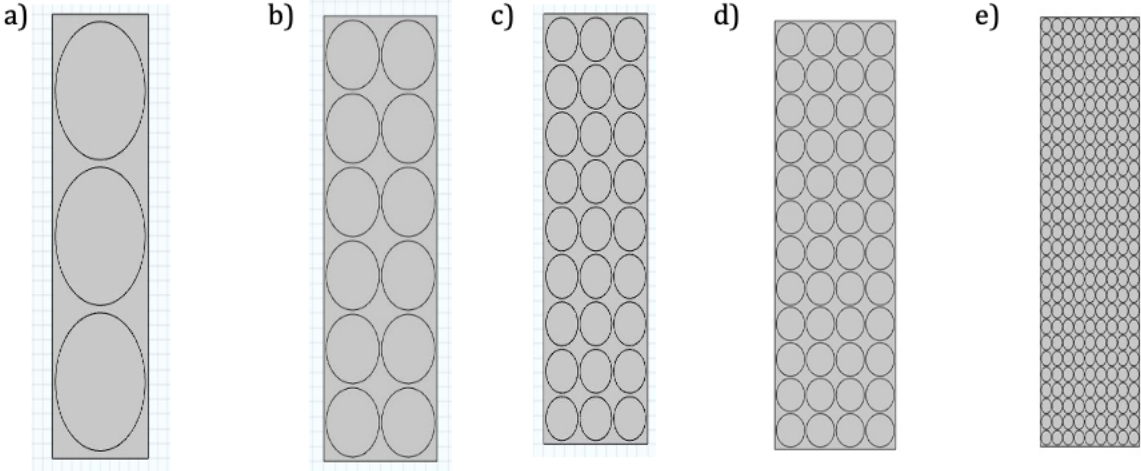
Figure 5.2: Geometries of regular packed circles in a 2D packed bed porosity (ϵ) of 0.316 at a) $\Lambda = 1.07$ b) $\Lambda = 2.14$ c) $\Lambda = 3.21$ d) $\Lambda = 4.28$ e) $\Lambda = 9.66$

The packed bed of four different porosities are designed with different aspect ratios as shown in the Figure 5.3 to see the effect of porosity on radial effective thermal conductivity.

The staggered packed bed of circles with three aspect ratios of porosity (ϵ) 0.316 shown in the Figure 5.4 as that of regular packing porosity as shown in the Figure 5.2 in order to see how packing pattern effects the radial heat transfer. In the staggered pattern, the distance between the circles is non-uniform.

29
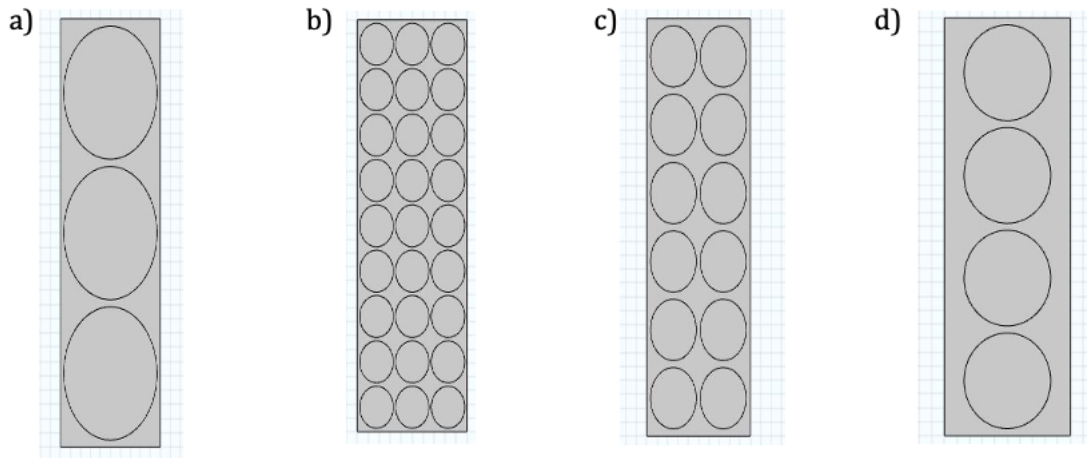
Figure 5.3: Geometries of regular packed circles in a 2D packed bed with different porosities (ϵ) a) $\epsilon = 0.316$ b) $\epsilon = 0.34$ c) $\epsilon = 0.387$ d) $\epsilon = 0.505$
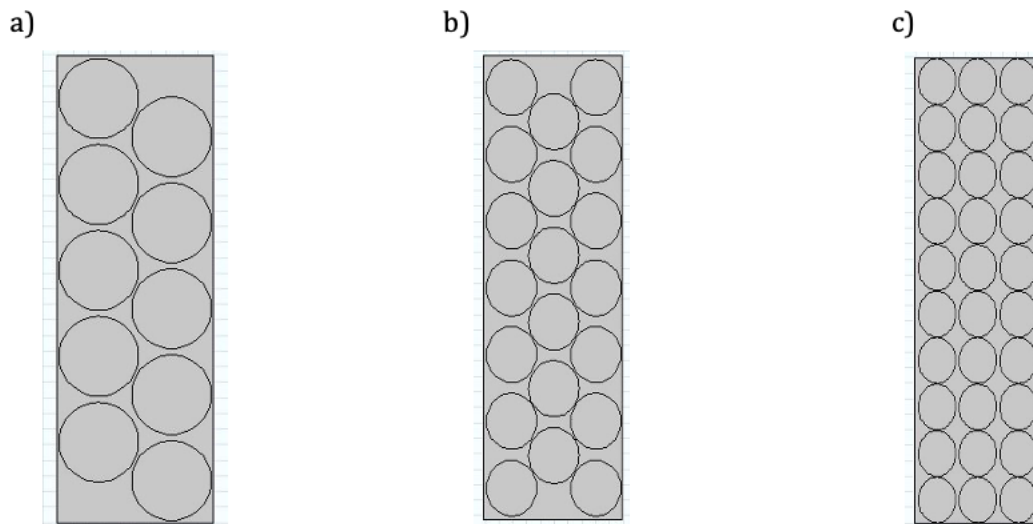
Figure 5.4: Geometries of staggered packed circles in a 2d packed bed porosity (ϵ) of 0.316 at a)$\Lambda= 1.95$ b) $\Lambda= 2.77$ c) $\Lambda= 3.39$

5.2.2 3D Packed Bed Design

A 3D packed bed is cylindrical in shape and has diameter of 40 mm. The reason for choosing cylindrical shape tube is to impose equal distribution of particles in a bed. The length of a bed varies based on the particle diameter.The bed is made of aluminum material and cylindrical heater made of copper placed in the middle of the bed surrounding by the solid sphere particles as shown in Figure 5.5 and Figure 5.6. The packed beds are designed in three different aspect ratios $(2 < \Lambda < 9)$ and solid sphere particles made up of brick, iron, steel, and aluminum.
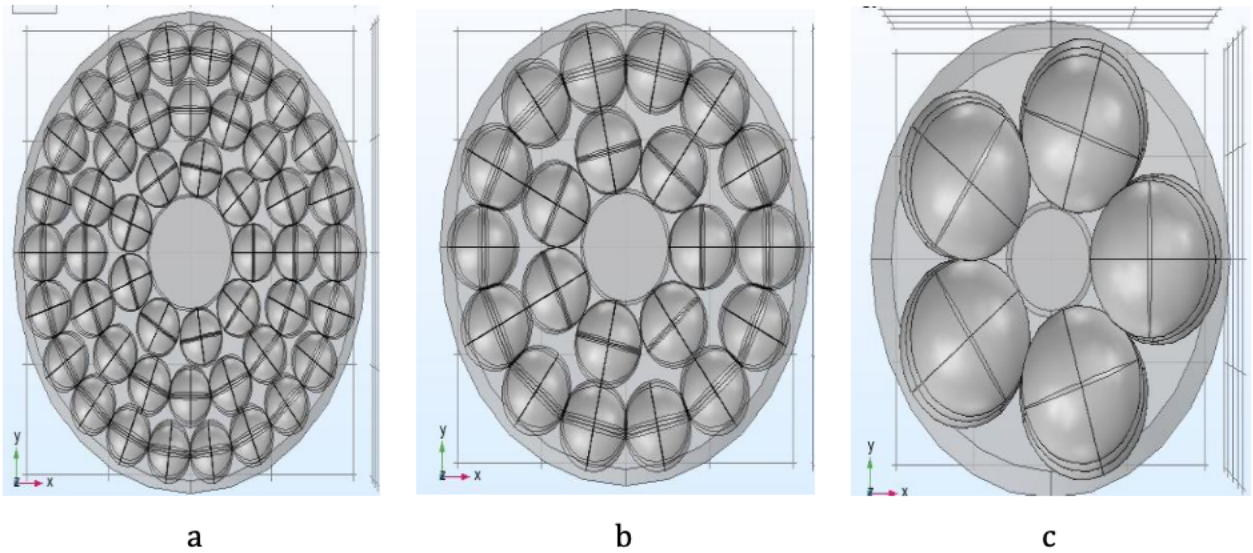
Figure 5.5: Geometries of radially packing spheres in a 3D packed bed a)Λ= 8.2 b) Λ= 5.46 c) Λ= 2.73

The structured packing arrangement is acceptable to obtain a better radial heat transfer in a packed bed because of particles are touching each other in a bed and there is a proper void age everywhere in a bed which could reduce large pressure drops. There are many types of structured packing arrangements such as FCC, BCC, SC, radial packing and hollow packing, but there are only two possible packing arrangements, which are radial packing and hollow packing due to design constraints of a bed with heater in the middle as shown in Figures 5.5 & 5.6.There is a gap of 0.5mm between the packing particles and packed bed wall in order to reduce meshing errors. All these models are designed and
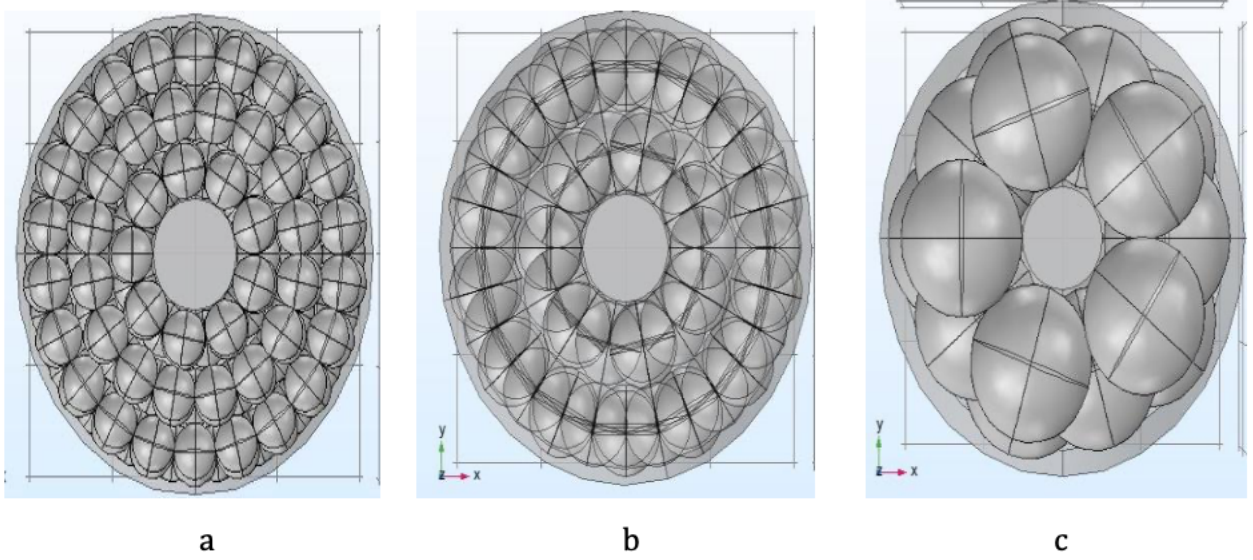
Figure 5.6: Geometries of hollow packing spheres in a 3D packed bed a)Λ= 8.2 b) Λ= 5.46 c) Λ= 2.73

simulated in COMSOL Multiphysics.

5.3   Initial and Boundary Conditions

Initial temperature conditions assumed to be ambient for analysis purpose.In 2D packed bed, the upper bed wall is subjected to natural convection (h=10 $\frac{W}{m^2-K}$), whereas the lower bed wall acts as a heat source which operates at 100 $\frac{W}{m^2}$. In 3D packed bed, the cylindrical heater operates at temperature of 400 K, 500 K, and 600 K. The packed bed walls subjected to natural convection.

The materials used for packing particles are brick, iron, steel, and aluminum. This simulation has conducted in non-stagnant laminar flow conditions of Re_P 0.5,1, 2, and 5.

5.3.1   Periodic Boundary Conditions

Considering real application of the problem, periodic boundary conditions are imposed at the inlet and outlet , which reduces computational effort and results in net heat trans-

fer in the radial direction only. The specified pressure drop, a requirement for periodic boundary conditions for Navier-Stokes equations, is used to control the Reynolds number of the flow.

$$P_{src} - P_{dst} = \Delta P$$

Periodic flow is assumed as a fully developed flow which has linear temperature and velocity profile along the length of a bed.

The temperature at the source and destination is the same which is $T_{src} = T_{dst}$.

The velocity field is depending on the pressure difference between two walls and pressure difference applied within the laminar flow region. Each pressure difference doesn't give the same velocity field and it is depending on the packing particle shape, packing particle diameter, packing bed length, particle spacing and porosity of a bed. Moreover, periodic boundary conditions provide a stable solution.

5.3.2   Computational Validation of Periodic Boundary Conditions

Figure 5.7: Rectangular duct with circles

A rectangular duct of 25mm length and 0.5mm height which is filled with circles of diameter 0.4 mm. The gap between the circles is 0.1mm. The inlet air operates at Peclet number (Pe) 150. Initial conditions are ambient,upper wall is subjected to temperature of 300 K, and lower wall is subjected to 400 K as shown in Figure 5.7.

A square duct of 0.5mm filled with a circle diameter of 0.4mm. The inlet of a duct act as a periodic source and outlet of a duct act as a periodic destination. The upper wall
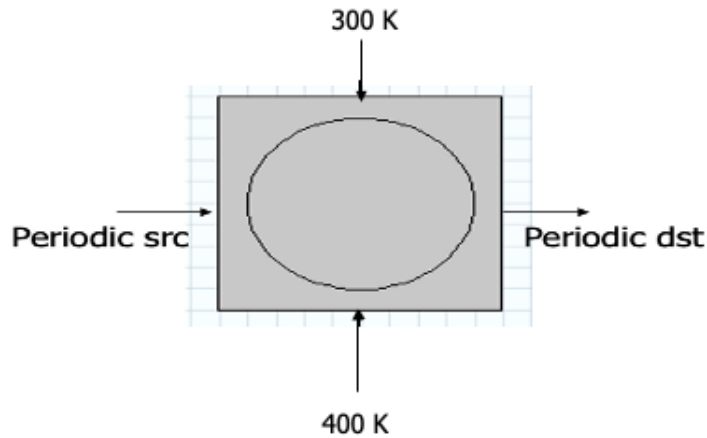
Figure 5.8: Periodic duct with one circle

operates at 300k and lower wall operates at 400k as shown in Figure 5.8.

These models are designed and simulated in COMSOL Multiphysics. A steady state conjugate heat transfer physics and Non-isothermal multiphysics are used and temperature values are recorded.

Figures 5.9 & 5.11 are showing the variation of temperature in radial direction. Figure 5.9 shows the comparison of radial temperature at the axial length of 22mm in Figure 5.7 with the periodic source in Figure 5.8. Similarly, Figure 5.11 shows the comparison of radial temperature at the axial length of 22.5mm in Figure 5.7 with the periodic destination in Figure 5.8.

Figure 5.10 shows that velocity profile becomes fully developed after certain length and Figure 5.9/5.11/5.12 clearly tells that temperature distribution becomes fully developed after certain length and exactly matches with the periodic domain. So, periodic boundary conditions are imposed for all models in this thesis.
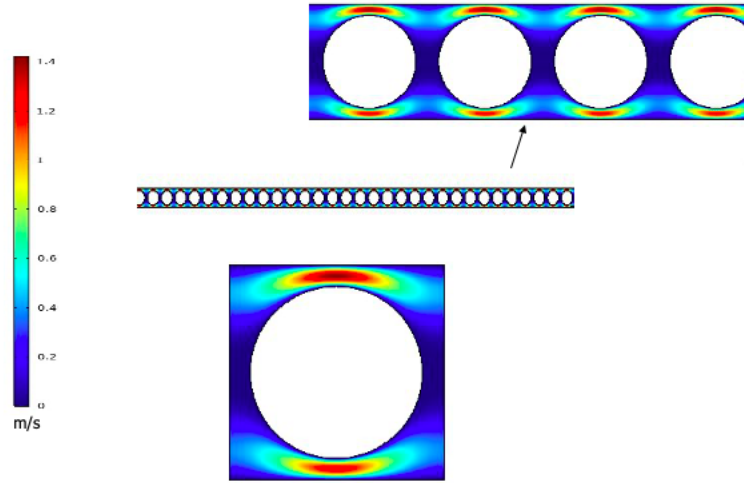
Figure 5.9: Velocity contour for rectangular duct with circles
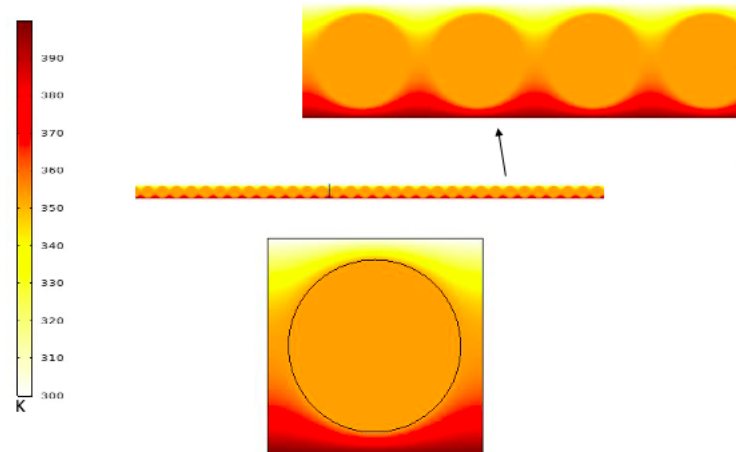
Figure 5.10: Temperature contour for rectangular duct with circles
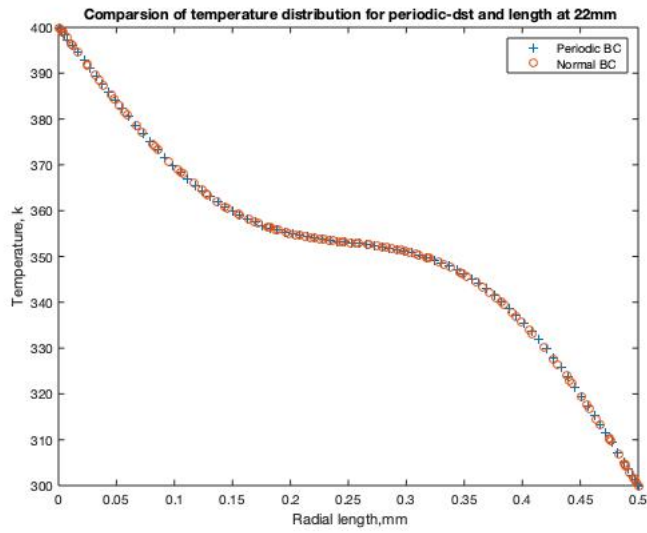
Figure 5.11: Comparison between normal BC and periodic BC at 22mm
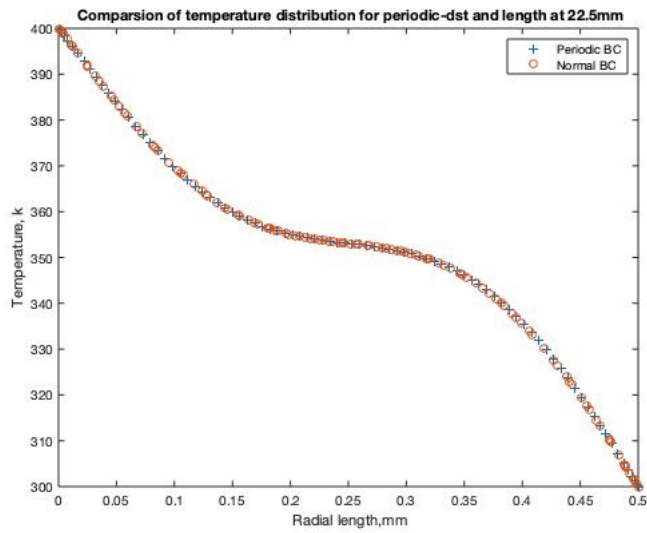
Figure 5.12: Comparison between normal BC and periodic BC at 22.5mm

36

5.4   Conjugate Heat Transfer and Fluid Flow

The conjugate heat transfer combines the heat transfer in solids and fluids. In general, solids dominate conduction and fluids dominate convection. Conjugate heat transfer observed in many application such as packed bed of spheres surrounding by a fluid (air in our case).This interface more precisely simulated where fluid properties depend on temperature and heat transfer in solids.

Usually, solids in a packed bed produce heat transfer due to conduction which is descried by a Fourier's law. The conduction equation for steady state heat transfer is:

$$q = -K \cdot (\nabla T)$$

Where, q is heat flux, K is thermal conductivity of a solid.

The fluid carries energy through the flow which is convection heat transfer. The heat transfer in fluids could also dominate either by convection or conduction depending upon the fluid type, flow region and thermal properties of a fluid[22]. The viscosity of fluid could also affect the heat transfer and it occurs more in turbulent region. If the density of a fluid become temperature dependent, the pressure term also affect the heat equation. Then heat equation including conduction would be:

$$\rho c_p u \cdot \nabla T = T(u \cdot \nabla P) + \tau : S + K \cdot \nabla T + Q$$

The conjugate heat transfer is used in many applications to minimize the heat losses due to low thermal conductivity of a fluids. The gases are using in many heat transfer devices because of low atomic weight.

In COMSOL, predefined couplings are available in both the directions. In other words, density is directly defined by reference temperature and reference pressure. The heat flux and the temperature become constant at solid/fluid interface. However, temperature field would change, when fluid in motion, the interface is far away and the solid and fluid are at same temperatures.The predefined couplings available for both laminar and turbulent flows.

The conjugate heat transfer has one of the major advantages is numerical stabilization which solves for conservation of mass, momentum, and energy in fluids and also conservation of energy in solids.

COMSOL also has fluid flow built-in feature along with conjugate heat transfer physics. Thermal insulation is default boundary condition for heat transfer and no slip is default boundary condition for fluid flow. The simulations are performed in low Reynolds numbers, so laminar flow is selected for analysis.

5.5   The Non-Isothermal Flow

The non-isothermal flow interface (COMSOL has default builtin feature) combines the heat equation and laminar flow in a fluid domain. The heat transfer process is fully coupled when non-isothermal physics is used.

The non-isothermal means temperature is not constant. The fluid properties, such as material properties, density and viscosity are changes according to the situation. In some cases, transportation of heat by the fluid itself would affect the temperature changes in the fluid. So, heat transfer and fluid flow coupling is interrelated to each other in many applications such as heat exchanges and chemical reactors. So, non-isothermal coupling is important when solving the heat transfer and fluid flow problem together.

5.6   Meshing of a Packed Bed

The mesh size is different for different aspect ratios since the gap between packing particles are different in each case. In 2D geometries, triangular and physics-controlled mesh is implied for all cases.

In 3D packed beds, combination of hexagonal and triangular mesh are implied to mesh curved surfaces properly.

5.6.1   2D Packed Bed Grid Independence Study

Table 5.1: 2D Grid independence study of aluminum circles with Λ=1.07 at T_H=400k

Mesh	Re_P	T_{avg}at wall 1
Fine	10	328.30
Extra Fine	10	328.32
Extremely Fine	10	328.32

The grid independence study from Table 5.1 shows that extra fine mesh and extremely fine mesh the same average temperature. So, extra mesh was chosen for all cases in this study in order to reduce computational time and obtain accurate results.

5.6.2   3D Packed Bed Grid Independence Study

Table 5.2: 3D Mesh independent study for radial packing of aluminum spheres with Λ =5.33 at T_H=400k

Mesh size	Re_P	T_{avg}at wall 1
1.2M	10	363.84
2.7M	10	363.89
3.8M	10	363.89

The grid independence study from Table 5.2 shows the average temperature for three different mesh sizes at Re_P=10 for radial packing with aluminum spheres. Mesh sizes of 2.7M cells and 3.1M cells giving the same average wall temperature which is also indicates 2.5M cells mesh is feasible in order to reduce computational time and accomplish correct results.
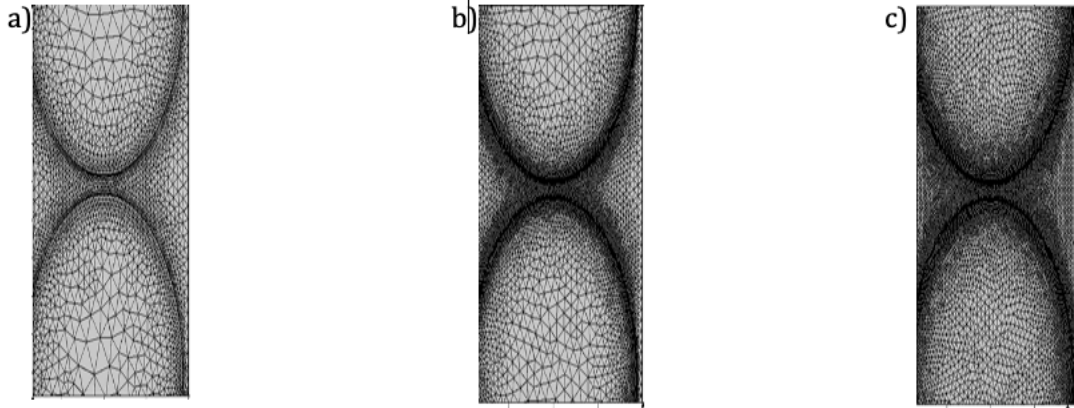
Figure 5.13: Meshing of a 2D packed bed of circles with $\Lambda = 1.07$ a) fine mesh b) extra fine mesh c) extremely fine mesh
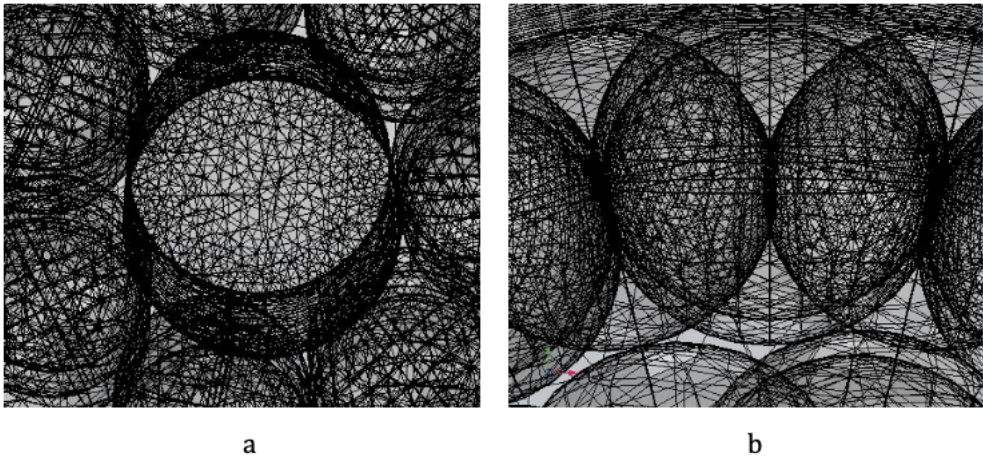
Figure 5.14: Meshing of a 3D packed bed of spheres with $\Lambda = 1.075.33$ a) Radial packing b) Hollow packing

Chapter 6

Results

6.1 2D Packed Bed Results

Initially, all computations are done in 2D to understand the problem better before committing to the time taking 3D simulations.The simulations are conducted within a laminar flow region $Re_P < 10$

6.1.1 Effect of Thermal Conductivity in a 2D Packed Bed
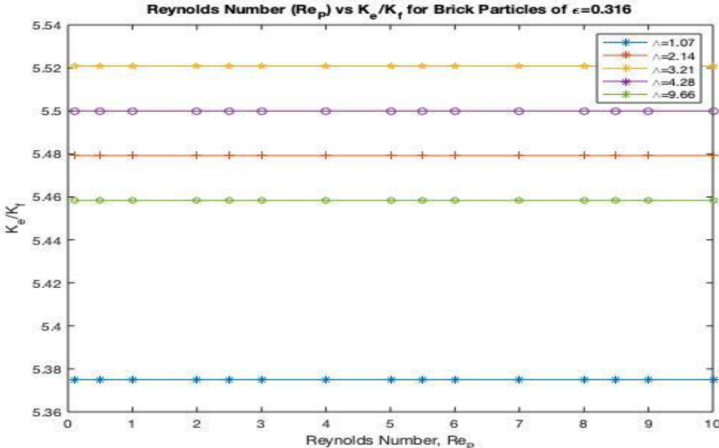
Figure 6.1: Variation of ETC in 2D packed bed with regular packing of brick circles of 5 different aspect ratios with the porosity $\epsilon = 0.316$ at heat flux 100 $\frac{w}{m^2}$

The $\frac{K_e}{K_f}$ is defines the radial heat transfer behavior in packed beds and which is non-

dimensional quantity. The aspect ratio of 3.21 producing high $\frac{K_e}{K_f}$ for both the brick and aluminum particles. In other hand, the aspect ratio of 1.07 producing less $\frac{K_e}{K_f}$ for both particles. The aspect ratio of 4.28 is producing $\frac{K_e}{K_f}$ is about the same as aspect ratio of 3.21 for both materials as shown in Figures 6.1 & 6.2. The conduction range between the circles and wall, gap between them, and size of a particles are creating this kind of scenario.
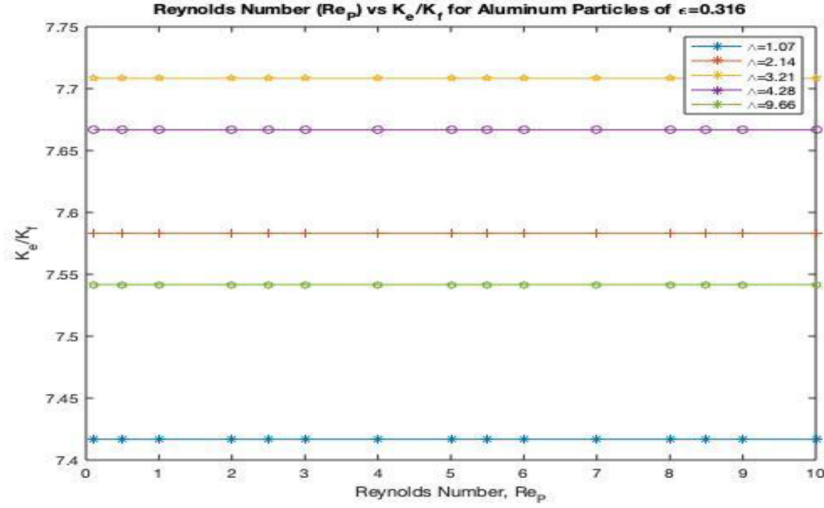
Figure 6.2: Variation of ETC in 2D packed bed with regular packing of aluminum circles of 5 different aspect ratios with the porosity $\epsilon = 0.316$ at heat flux 100 $\frac{w}{m^2}$

The effect of thermal conductivity of packing materials shows high impact on $\frac{K_e}{K_f}$. Figure 6.1 shows that brick circles producing highest $\frac{K_e}{K_f}$ of 5.52 and Figure 6.2 shows that aluminum circles producing $\frac{K_e}{K_f}$ is about 7.71. The $\frac{K_e}{K_f}$ is constant as Reynolds number is increasing in the laminar flow region for each aspect ratio and each material.

6.1.2 Effect of Porosity in a 2D Packed Bed

The $\frac{K_e}{K_f}$ is increasing as porosity decreases. The porosity of 0.316 is producing highest $\frac{K_e}{K_f}$ is about 7.5 and the porosities of 0.387 and 0.505 is producing lowest $\frac{K_e}{K_f}$ is about 5.5. There is a large difference in $\frac{K_e}{K_f}$ between $\epsilon = 0.34$ & 0.387 when compared to $\epsilon= 0.316$ & 0.34 as shown in Figure 6.3. The $\frac{K_e}{K_f}$ is constant as Reynolds number is increasing in the laminar flow region for each porosity because there is no circulation effect and no secondary

42
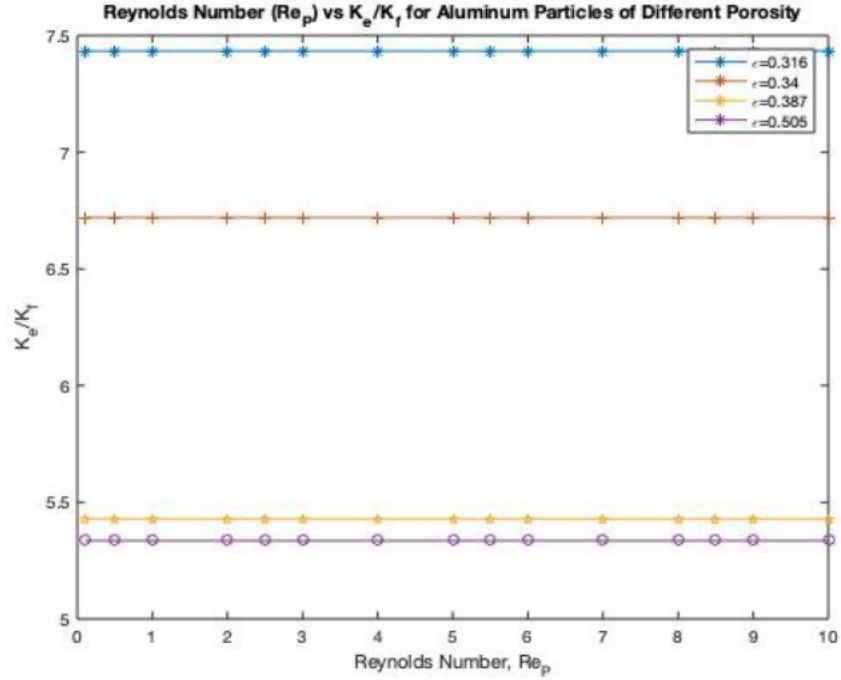
Figure 6.3: Packed bed of aluminum circles for 4 porosity designs at heat flux 100 $\frac{w}{m^2}$

flow when Re in an order of ones.

Table 6.1: Variation of $\frac{K_e}{K_f}$ packed bed of circles with different materials and different porosity values at heat flux 100 $\frac{w}{m^2}$ and Re_p 10

Packing Material	$\epsilon= 0.316$	$\epsilon=0.34$	$\epsilon=0.387$	$\epsilon=0.505$
Brick	5.413	5.055	4.385	4.109
Glass	6.546	6.005	5.000	4.809
Steel	7.282	6.699	5.434	5.321
Iron	7.420	6.710	5.434	5.327
Aluminum	7.433	6.720	5.434	5.335

The Table 6.1 showing that as porosity is increasing, ETC is decreases for each and every material. The difference of $\frac{K_e}{K_f}$ between the ϵ=0.316 and ϵ=0.505 for aluminum particles is about 2. However, the difference of $\frac{K_e}{K_f}$ between the ϵ=0.316 and ϵ=0.505 for brick particles is about 1.3. It's clearly indicated that there is always effect of thermal conductivity on radial heat transfer. The porosity of 0.316 would consider to be best choice and feasible to obtain good heat transfer performance.

The difference of $\frac{K_e}{K_f}$ between the brick and aluminum particles for porosity of 0.316 is about 2. However, the difference of $\frac{K_e}{K_f}$ between the brick and aluminum particles for porosity of 0.316 is about 1.2. It's clearly demonstrated that the porosity is shows high impact on the radial heat transfer. So, the packing material conductivity and porosity are some of the major parameters which shows effect on ETC.

6.1.3 Effect of Staggered Packing Arrangement in a 2D Packed Bed

Table 6.2: Variation of $\frac{K_e}{K_f}$ staggered packing of circles with different materials and different aspect ratios of same porosity at heat flux 100 $\frac{w}{m^2}$ and Re_p 10

Packing Material	Λ= 1.95	Λ=2.77	Λ= 3.39
Brick	5.112	5.183	7.174
Glass	6.037	6.291	10.625
Steel	6.704	7.179	14.212
Iron	6.716	7.195	14.287
Aluminum	6.725	7.208	14.341

Table 6.2 shows that packing structure, aspect ratio and thermal conductivity of packing material are crucial parameters to ETC. The difference of $\frac{K_e}{K_f}$ between the staggered packing of brick and aluminum is about 1.5 for aspect ratio 1.95. However, the difference of $\frac{K_e}{K_f}$ between the staggered packing of brick and aluminum is about 7 for aspect ratio 3.39 which is almost 5 times more than aspect ratio of 1.95. The $\frac{K_e}{K_f}$ value of brick packing with aspect ratio 3.39 is more than aluminum packing with aspect ratio 1.95 and almost equal to aluminum packing with aspect ratio 2.77.

6.1.4 Comparison between Regular Packing and Staggered Packing in a 2D Packed Bed

	Brick	Glass	Steel	Iron	Aluminum
■ Regular packing	5.414	6.548	7.283	7.420	7.434
■ Staggered Packing	7.175	10.625	14.213	14.288	14.342
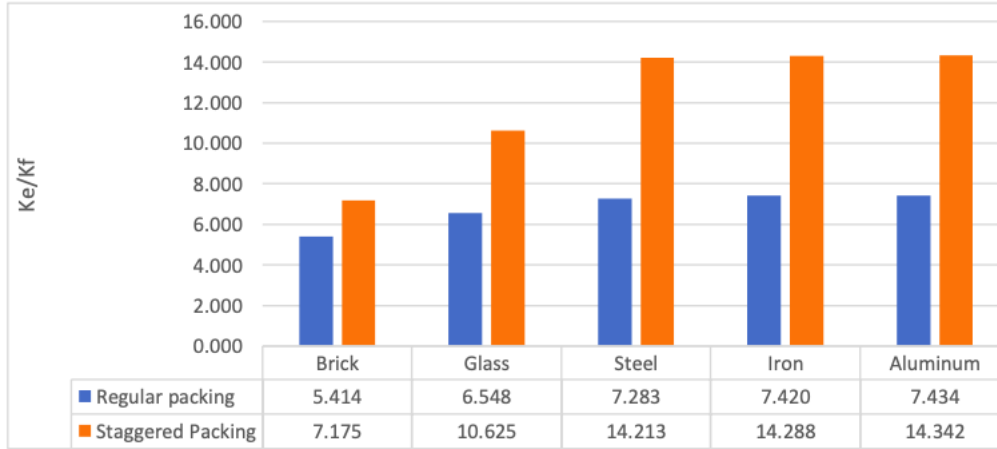
Figure 6.4: Highest ETC comparison for regular and staggered packing

Figure 6.4 shows the variation of ETC for both regular and staggered packing of circular particles at $Re_P 10$ for porosity of 0.316. The staggered packing with aspect ratio of 3.39 producing very high $\frac{K_e}{K_f}$ for both the brick and aluminum when compare with other two aspect ratios. Similarly, the aspect ratio of 1.95 producing less $\frac{K_e}{K_f}$ for both the brick and aluminum.

The effect of thermal conductivity of packing materials shows high impact on $\frac{K_e}{K_f}$. Table 6.1/6.2 shows that brick circles producing highest $\frac{K_e}{K_f}$ of 7.2 and aluminum circles producing $\frac{K_e}{K_f}$ is about 14.5. The $\frac{K_e}{K_f}$ is constant as Reynolds number is increasing in the laminar flow region for each aspect ratio and each material regardless of packing structure.

The regular aluminum packing material with aspect ratio of 3.21 is producing $\frac{K_e}{K_f}$ of 7.71 as shown in the Table 6.1/6.2. However, staggered aluminum packing of aspect ratio of 3.39 producing $\frac{K_e}{K_f}$ of 14.5 as shown in the Figure 4.3. There is no significant difference between steel and aluminum particles. It is clearly stating that packing structure is also one of the major parameters to enhance the radial heat transfer.

6.1.5   Temperature Contours for a 2D Packed Bed

The Figure 6.5 showing that lower wall has the maximum average temperature of 345K for brick and 328K for aluminum. The upper wall temperature is same in both cases which is 310 K. The difference between the lower wall and upper wall should be less in order to maximize the ETC in a 2D packed bed.

Similarly, the lower wall has the maximum average temperature of 355 K for brick and 345 K for aluminum. The upper wall temperature is same in both cases which is 310K as shown in Figure 6.6. The difference between the lower wall and upper wall should be less in order to maximize the radial heat transfer in a 2D packed bed. So, figure 4.5 and figure 4.6 are clearly shows the effect of packing material thermal conductivity on radial heat transfer regardless of packing arrangement.
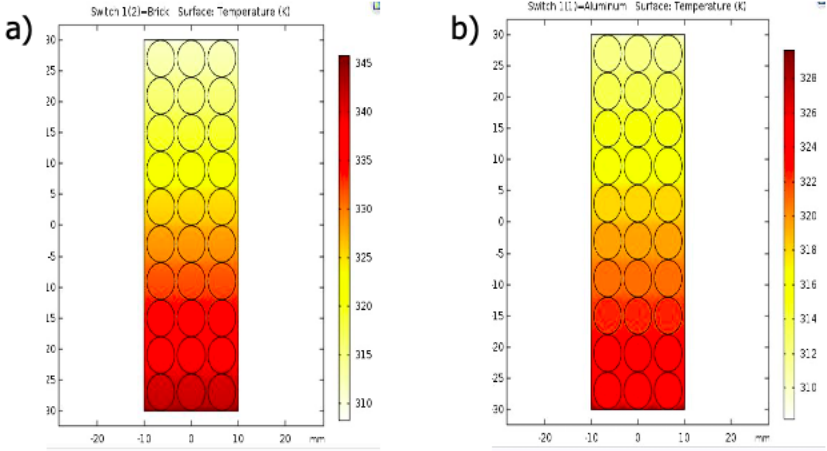
Figure 6.5: Temperature contours for staggered packing with aspect ratio of 3.39 at heat flux 100 $\frac{w}{m^2}$ a)Brick b)Aluminum
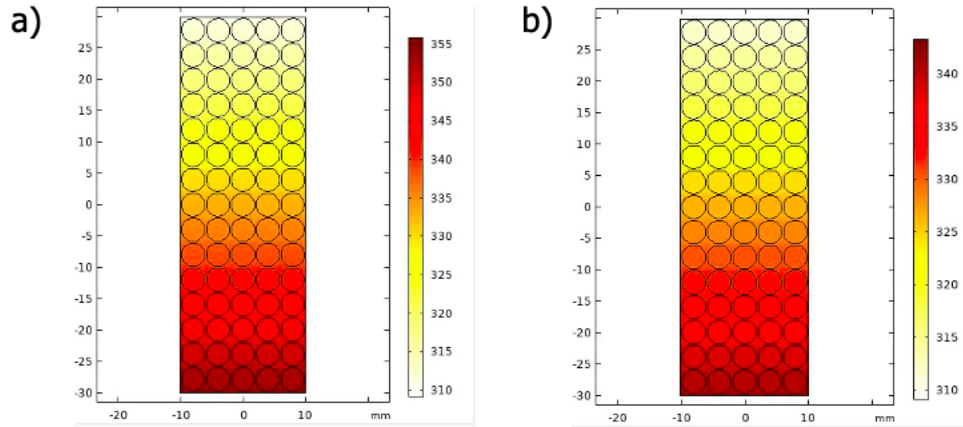
Figure 6.6: Temperature contours for regular packing with aspect ratio of 3.21 at heat flux 100 $\frac{w}{m^2}$ a)Brick b)Aluminum

6.1.6 Velocity Contours for a 2D Packed Bed
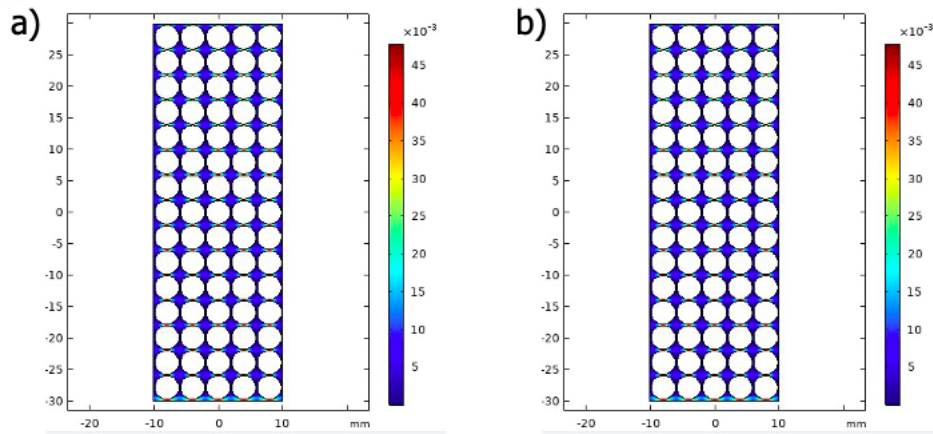
Figure 6.7: Velocity contours for regular packing with aspect ratio of 3.21 at Re_P=1 a)Brick b)Aluminum

The maximum velocity is about 0.045 $\frac{m}{s}$ and minimum velocity is about 0.005 $\frac{m}{s}$ for both brick and aluminum packed circles shown in figure 6.7. So,velocity distribution is same for all cases regardless of packing material. The velocity distribution only vary with packing material diameter, aspect ratio, and packing arrangement.

47

6.2 3D Packed Bed Results

The 2D packed bed results provided good understanding of a problem. It also provided nature of the results on how different parameters effects ETC of a packed bed. In 2D cases, mesh properties and boundary conditions are different. Moreover, forces and momentum are neglected in third direction. However, 3D simulations are computationally burden but sophisticated system, it is important to obtain accurate and realistic values.

6.2.1 Effect of Heater Temperature in a 3D Packed Bed with Radial Packing Arrangement
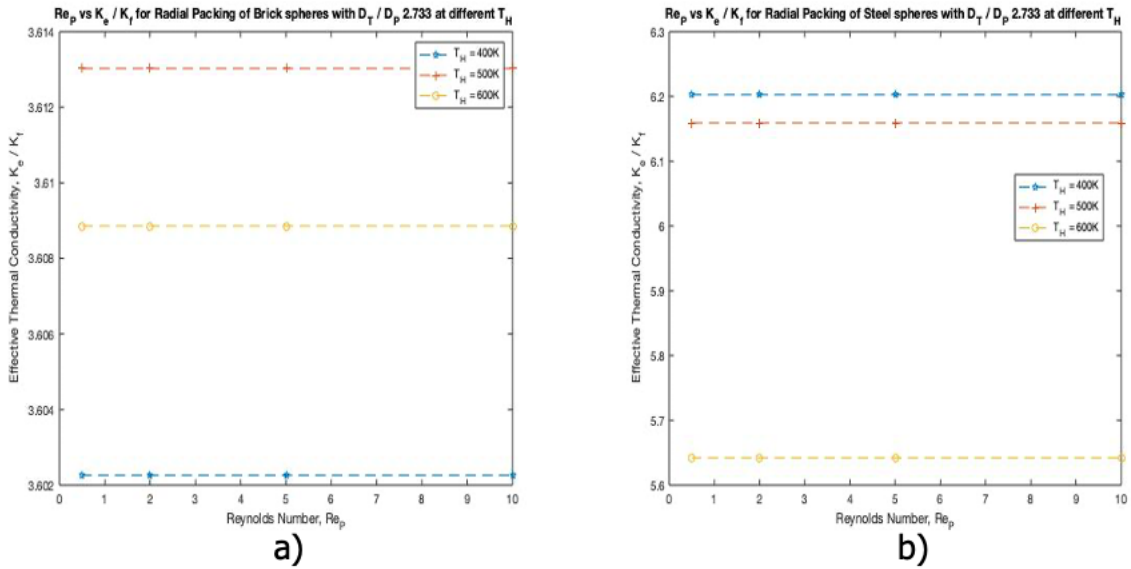
a)   b)

The heater temperature T_H of 500 K producing highest $\frac{K_{eff}}{K_f}$ and heater temperature of 400 K producing lowest $\frac{K_{eff}}{K_f}$ when compared to other T_H. For iron, steel, and aluminum packing spheres (showing in Figures 6.8 (b),(c), and(d)) are producing highest $\frac{K_{eff}}{K_f}$ at T_H 400 K and lowest at T_H 600 K as shown in Figure 6.8. Since the heater temperature inversely is propositional to ETC. However, it will depend on bulk temperature, wall temperature and conduction from the heater to the wall for some material where thermal conductivity is less.

c)

d)
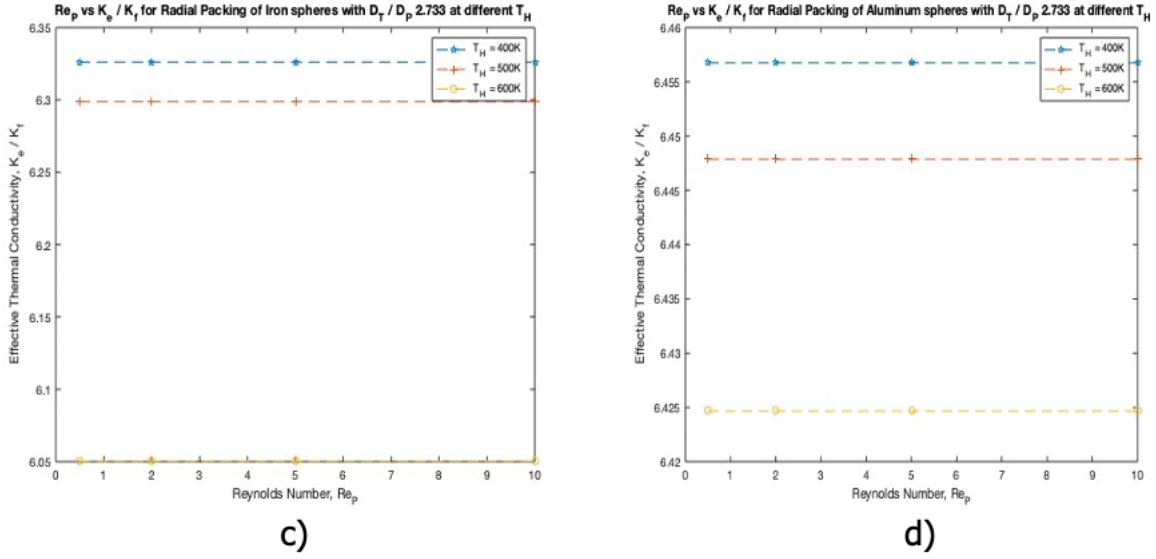
Figure 6.8: Variation of ETC in 3D packed bed with radial packing of spheres of 3 different heater temperatures with the aspect ratio (Λ)of 2.73 a)Brick b)Iron c)Steel d)Aluminum

The $\frac{K_{eff}}{K_f}$ is constant for all Reynolds numbers within a laminar flow region in packed beds since Reynolds numbers are just in a order of ones which can't create more separation, re-circulation and secondary flows to effect radial heat transfer.

The ETC is varying with a material type at same temperatures shown in Tables 6.3& 6.4. It is also showing that heater temperature at 600 K of brick packing spheres are producing highest $\frac{K_{eff}}{K_f}$ and heater temperature of 400 K producing lowest $\frac{K_{eff}}{K_f}$ when compared to other T_H. The iron, steel, and aluminum packing spheres are producing highest $\frac{K_{eff}}{K_f}$ at T_H 400 K and lowest at T_H 600 K. This pattern is happening in both the aspect ratios of 5.466 & 8.2. So, all these together shows the impact of heater temperature on ETC for different materials and aspect ratios.

6.2.2 Effect of Thermal Conductivity of a Packing Material in a 3D Packed Bed with Radial Packing Arrangement

Figure 6.8 shows that the aspect ratio of 2.733 with aluminum packing is producing highest $\frac{K_{eff}}{K_f}$ is about 6.65 and with brick packing is producing lowest $\frac{K_{eff}}{K_f}$ is about 3.6. The steel

Table 6.3: Variation of ETC in 3D packed bed with radial packing spheres of 3 different heater temperatures with the aspect ratio (Λ)of 5.46

| Packing Material	$\frac{K_{eff}}{K_f}$ at T_H 400 K	$\frac{K_{eff}}{K_f}$ at T_H 500 K	$\frac{K_{eff}}{K_f}$ at T_H 600 K
Brick	3.305	3.165	**3.31**
Steel	**6.93**	6.83	6.73
Iron	**7.23**	7.14	7.07
Aluminum	**7.52**	7.48	7.36

Table 6.4: Variation of ETC in 3D packed bed with radial packing spheres of 3 different heater temperatures with the aspect ratio (Λ)of 8.2

Packing Material	$\frac{K_{eff}}{K_f}$ at T_H 400 K	$\frac{K_{eff}}{K_f}$ at T_H 500 K	$\frac{K_{eff}}{K_f}$ at T_H 600 K
Brick	3.424	3.438	**3.443**
Steel	**5.25**	5.175	5.12
Iron	**5.65**	5.55	5.45
Aluminum	**6.7**	6.55	6.43

packing and iron packing are producing $\frac{K_{eff}}{K_f}$ is about the same of 6.3.

The aspect ratio of 5.46 with aluminum packing is producing highest $\frac{K_{eff}}{K_f}$ is about 7.5 and with brick packing is producing lowest $\frac{K_{eff}}{K_f}$ is about 3.3. The steel packing is producing $\frac{K_{eff}}{K_f}$ is about 7 and iron packing is producing is about 7.2 as shown in Table 6.3.

The aspect ratio of 8.2 with aluminum packing is producing highest $\frac{K_{eff}}{K_f}$ is about 6.7 and with brick packing is producing lowest $\frac{K_{eff}}{K_f}$ is about 3.44. The steel packing is producing $\frac{K_{eff}}{K_f}$ is about 5.25 and iron packing is producing is about 5.65 as shown in Table 6.4.

The packing material of aluminum spheres producing about twice amount of $\frac{K_{eff}}{K_f}$ when compared to brick particles in all cases. The packing spheres of steel & iron spheres behaving same as a aluminum spheres. The conduction of solid spheres is dominant in packed beds when operates within a laminar flow region. This is clearly explains how high impact thermal conductivity of a packing material showing on radial heat transfer in packed beds.

50

6.2.3 Effect of Aspect Ratio in a 3D Packed Bed with Radial Packing Arrangement

The aspect ratio of 2.733 is producing highest ETC and aspect ratio of 5.466 is producing lowest ETC for brick packing particles. The aspect ratio of 5.466 is producing highest ETC and aspect ratio of 8.2 producing lowest for steel and iron packing particles. The aspect ratio of 5.466 is producing highest ETC and aspect ratio of 2.733 for aluminum packing particles as shown in Table 6.5.

Table 6.5: Variation of highest ETC in 3D packed bed with radial packing spheres of 3 different aspect ratios and for 4 different materials

Packing Material	$\frac{K_{eff}}{K_f}$ with Λ =2.733	$\frac{K_{eff}}{K_f}$ with Λ =5.466	$\frac{K_{eff}}{K_f}$ with Λ =8.2
Brick	**3.6**	3.3	3.425
Steel	6.2	**6.93**	5.25
Iron	6.35	**7.23**	5.65
Aluminum	6.43	**7.52**	6.7

According to the Ergun's equation, pressure is drop high when particle diameter is low. In this radial packing arrangement, the =8.2 is producing less ETC since it doesn't influence the flow in radial direction due to low particle diameter and higher pressure drop. Similarly, the =2.733 producing better ETC when compared to the =8.2, but the gap between the spheres near the wall is high which might cause less conduction in radial direction. Finally, the aspect ratio of 5.66 is good to achieve better radial heat transfer in a packed bed where it maintains proper pressure drop, proper gap between particles and good conduction near the wall. So, the aspect ratio is also one of the major parameters while designing a packed bed for required application.

6.2.4 Temperature Contours for a 3D Packed Bed in a Radial Packing Arrangement

The Figure 6.9 (b) shows the high radial temperature distribution, where as Figure 6.9 (c) shows the less radial temperature distribution because of voids between the spheres are large. Similarly, Figure 6.10 (c) shows the high radial temperature distribution, where

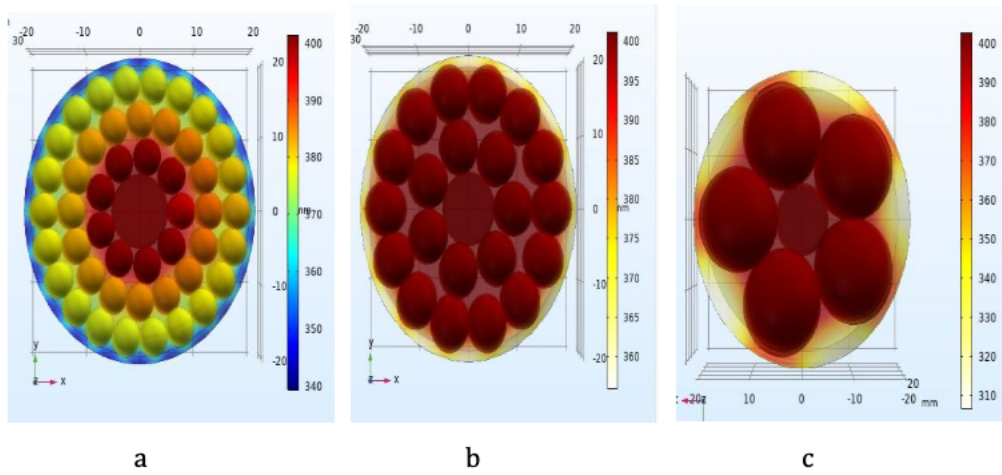Figure 6.9: Temperature contours for radially packed aluminum spheres in a packed bed at Re_P10 a) $\Lambda =8.2$ b) $\Lambda=5.46$ c) $\Lambda =2.733$
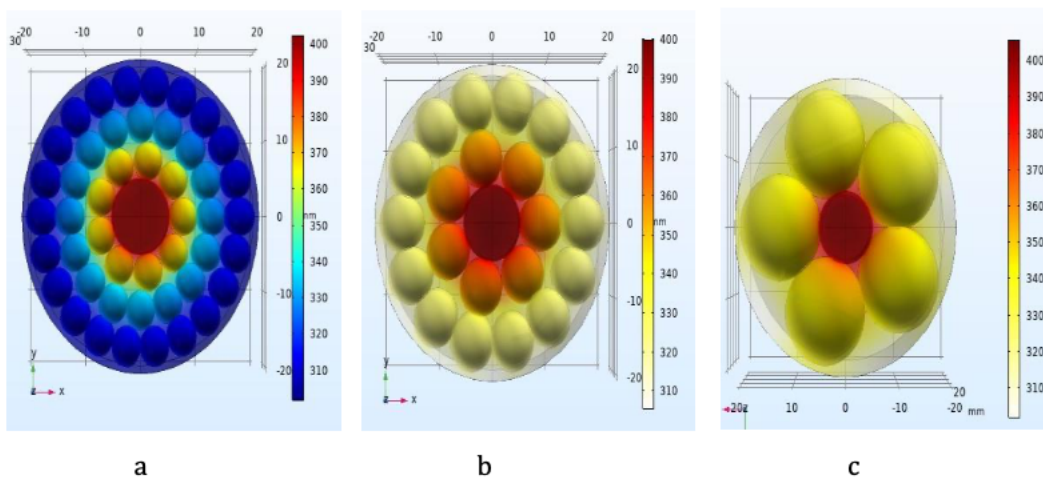
Figure 6.10: Temperature contours for radially packed brick spheres in a packed bed at Re_P10 a) $\Lambda =8.2$ b) $\Lambda=5.46$ c) $\Lambda =2.733$

as Figure 6.10 (b) shows the less radial temperature distribution because of the packing material properties. So, packing arrangement and material properties are important to obtain better heat transfer performance.

6.2.5 Effect of Heater Temperature in a 3D Packed Bed with Hollow Packing Arrangement

The heater temperature T_H of 500 K producing highest $\frac{K_{eff}}{K_f}$ and heater temperature of 400 K producing lowest $\frac{K_{eff}}{K_f}$ when compared to other T_H for brick particles as shown in Figure 6.11 (a). For iron, steel, and aluminum packing spheres (shown in Figures 6.11 (b),(c), and(d)) are producing highest $\frac{K_{eff}}{K_f}$ at T_H 400 K and lowest at T_H 600 K. The $\frac{K_{eff}}{K_f}$ is constant for all Reynolds numbers within a laminar flow region in packed beds since Reynolds numbers are just in a order of ones which can't create more separation, re-circulation and secondary flows to effect radial heat transfer.
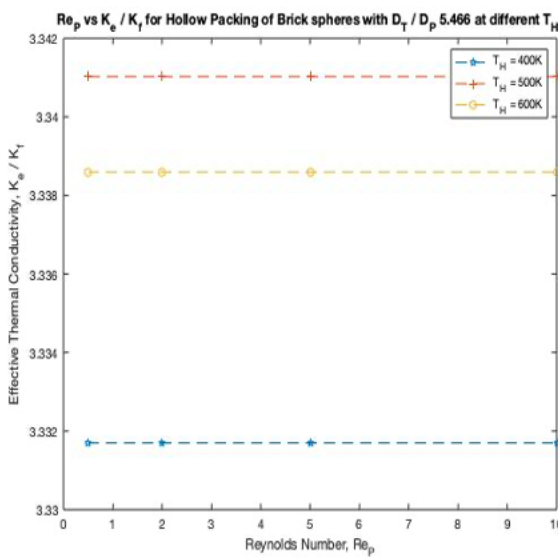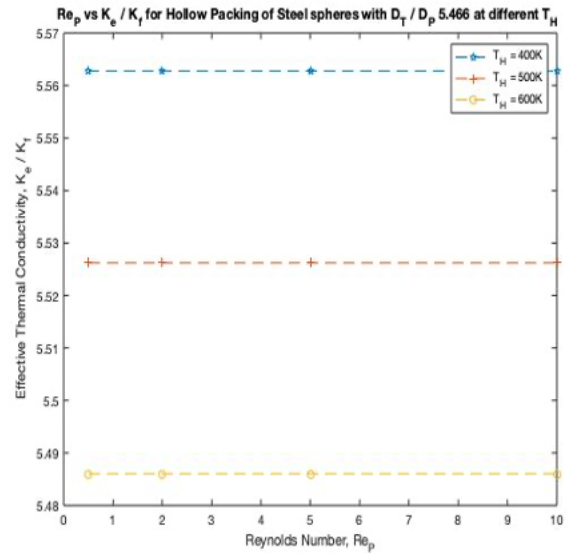
a)   b)

Table 6.6 showing that when brick packing spheres are exposing to a heater temperature of 500 K which will produce highest $\frac{K_{eff}}{K_f}$ and heater temperature of 400 K producing lowest $\frac{K_{eff}}{K_f}$ when compared to other T_H. The iron and steel packing spheres are produc-
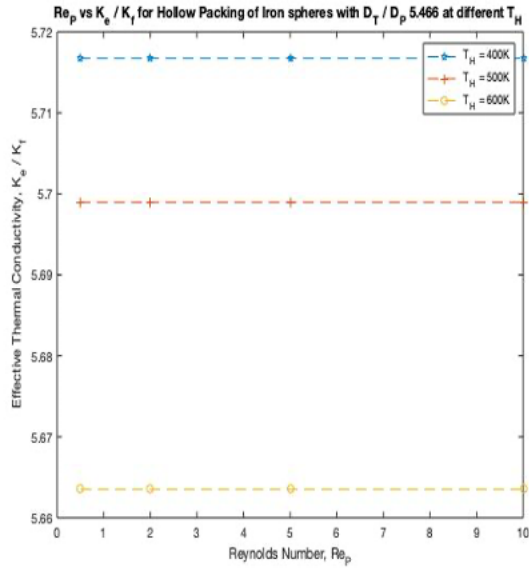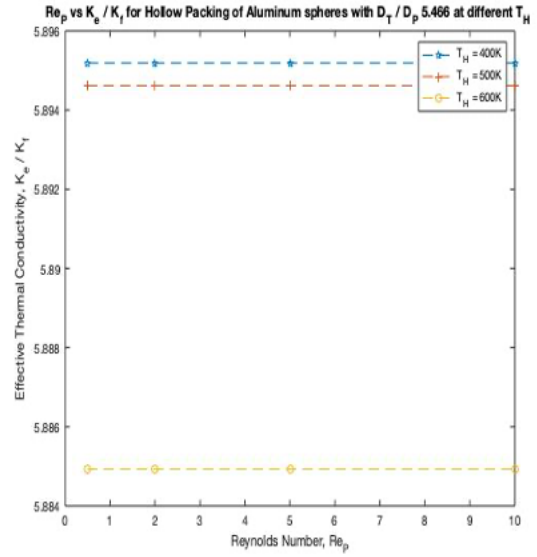
Figure 6.11: Variation of ETC in 3D packed bed with hollow packing of spheres of 3 different heater temperatures with the aspect ratio (Λ)of 5.466 a)Brick b)Iron c)Steel d)Aluminum

ing highest $\frac{K_{eff}}{K_f}$ at T_H 400 K and lowest at T_H 600 K. Aluminum packing spheres are producing highest $\frac{K_{eff}}{K_f}$ at T_H 500k and lowest at T_H 400 K. However, it will depend on bulk temperature, wall temperature and conduction from the heater to the wall for some material where thermal conductivity is less.

Table 6.7 showing that heater temperature at 500 K for brick spheres producing highest $\frac{K_{eff}}{K_f}$ and heater temperature of 600 K producing lowest $\frac{K_{eff}}{K_f}$ when compared to other T_H. The iron steel and aluminum packing spheres are producing highest $\frac{K_{eff}}{K_f}$ at T_H 400 K and lowest at T_H 600 K. So, all these together shows the impact of heater temperature on ETC for different materials and aspect ratios. However, there is only negligible amount of change for all heater temperatures.

Table 6.6: Variation of ETC in 3D packed bed with hollow packing spheres of 3 different heater temperatures with the aspect ratio (Λ)of 2.773

Packing Material	$\frac{K_{eff}}{K_f}$ at T_H 400 K	$\frac{K_{eff}}{K_f}$ at T_H 500 K	$\frac{K_{eff}}{K_f}$ at T_H 600 K
Brick	3.592	**3.6**	3.596
Steel	**6.205**	6.16	6.115
Iron	**6.325**	6.295	6.27
Aluminum	6.43	**6.445**	6.435

Table 6.7: Variation of ETC in 3D packed bed with hollow packing spheres of 3 different heater temperatures with the aspect ratio (Λ)of 8.2

Packing Material	$\frac{K_{eff}}{K_f}$ at T_H 400 K	$\frac{K_{eff}}{K_f}$ at T_H 500 K	$\frac{K_{eff}}{K_f}$ at T_H 600 K
Brick	3.52	**3.58**	3.41
Steel	**5.02**	4.99	4.93
Iron	**5.255**	5.195	5.165
Aluminum	**5.9**	5.82	5.76

6.2.6 Effect of Thermal Conductivity of a Packing Material in a 3D Packed Bed with Hollow Packing Arrangement

The aspect ratio of 5.466 with aluminum packing is producing highest $\frac{K_{eff}}{K_f}$ is about 5.895 and with brick packing is producing lowest $\frac{K_{eff}}{K_f}$ is about 3.34. The steel packing and iron packing are producing $\frac{K_{eff}}{K_f}$ is about the same of 5.7 as shown in Figure 6.11.

The aspect ratio of 2.773 with aluminum packing is producing highest $\frac{K_{eff}}{K_f}$ is about 6.43 and with brick packing is producing lowest $\frac{K_{eff}}{K_f}$ is about 3.3. The steel and iron packing are producing $\frac{K_{eff}}{K_f}$ is about 6.3 as shown in Table 6.6.

The aspect ratio of 8.2 with aluminum packing is producing highest $\frac{K_{eff}}{K_f}$ is about 5.9 and with brick packing is producing lowest $\frac{K_{eff}}{K_f}$ is about 3.58. The steel packing is producing $\frac{K_{eff}}{K_f}$ is about 5 and iron packing is producing is about 5.25 as shown in Table 6.7.

The packing material of aluminum spheres producing more than 150% of $\frac{K_{eff}}{K_f}$ when compared to brick particles in all cases. The packing spheres of steel & iron spheres

behaving same as a aluminum spheres. The conduction of solid spheres is dominant in packed beds within a laminar flow region. This is clearly explains how high impact thermal conductivity of a packing material showing on radial heat transfer in packed beds.

6.2.7 Effect of Aspect Ratio in a 3D Packed Bed with Hollow Packing Arrangement

The aspect ratio of 2.733 is producing highest ETC. The aspect ratio of 8.2 is producing lowest ETC for steel, iron and aluminum materials and aspect ratio of 5.466 producing lowest $\frac{K_{eff}}{K_f}$ for brick particles as shown in Table 6.8. So, the aspect ratio 2.733 is feasible for hollow packing arrangement of spheres in a packed bed to achieve better radial heat transfer.

Table 6.8: Variation of highest ETC in 3D packed bed with hollow packing spheres of 3 different aspect ratios and for 4 different materials

Packing Material	$\frac{K_{eff}}{K_f}$ with Λ =2.733	$\frac{K_{eff}}{K_f}$ with Λ =5.466	$\frac{K_{eff}}{K_f}$ with Λ =8.2
Brick	**3.6**	3.33	3.57
Steel	**6.2**	5.6	5.0
Iron	**6.3**	5.7	5.2
Aluminum	**6.45**	5.9	5.9

As mentioned earlier, pressure is drop less when particle diameter is high. The pressure drop is less in hollow packing arrangement when compare with other packing arrangements due to the arrangement and gap between the particles are less. So, in this hollow packing arrangement, the Λ =8.2 and Λ = 5.466 are producing less ETC when compare with Λ =2.733. The reason is that bigger spheres are occupied in high volume near the wall which means higher conduction produces better radial heat transfer.

6.2.8 Temperature Contours for a 3D Packed Bed in a Hollow Packing Arrangement
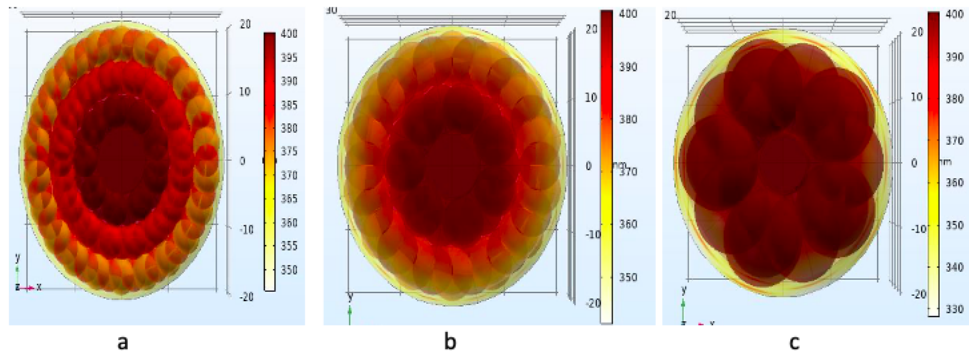
Figure 6.12: Temperature contours for hollow packed aluminum spheres in a packed bed at $Re_P 10$ a) Λ =8.2 b) Λ=5.46 c) Λ =2.733
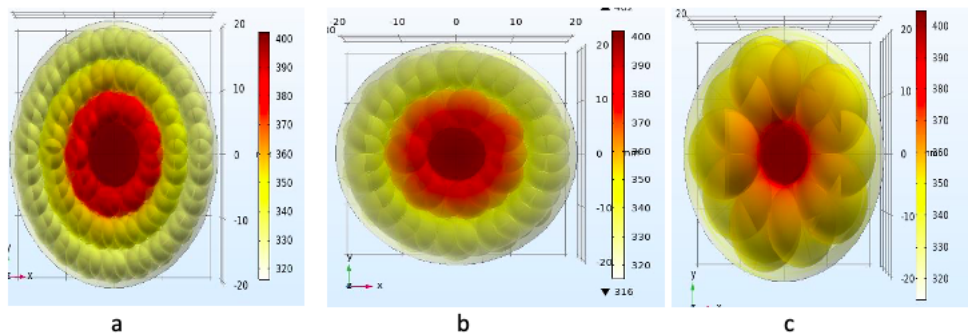
Figure 6.13: Temperature contours for hollow packed brick spheres in a packed bed at $Re_P 10$ a) Λ =8.2 b) Λ=5.46 c) Λ =2.733

The Figure 6.12 (c) represents the high radial temperature distribution because it has larger distribution of particles in hollow manner, where as Figures 6.12 (a) & (b) shows the less radial temperature distribution. Similarly, Figure 6.13 (c) shows the high radial temperature distribution where as Figures 6.13 (a) & (b) shows the less radial temperature distribution because of lesser distribution of particles.

6.2.9 Comparison between Radial Packing and Hollow Packing in a 3D Packed Bed
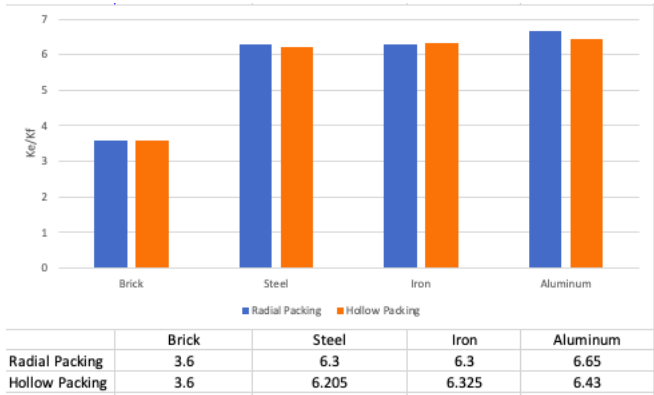
Figure 6.14: Highest ETC comparison for radial and hollow packing with aspect ratio of 2.733
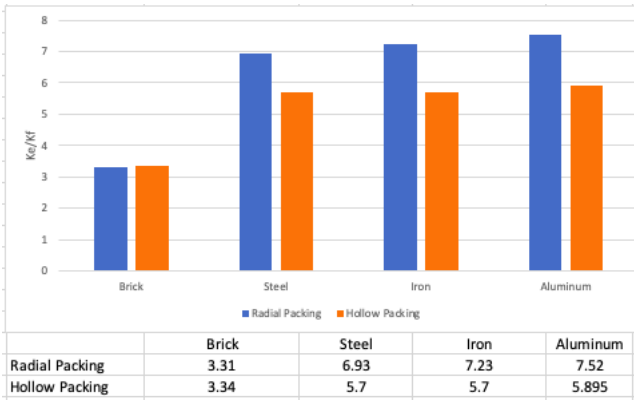
Figure 6.15: Highest ETC comparison for radial and hollow packing with aspect ratio of 5.466

The aspect ratio of 2.733 producing about the same $\frac{K_e}{K_f}$ values for all materials regardless of packing arrangement as shown in Figure 6.14. The steel, iron and aluminum spheres have almost same ETC in both packing arrangements.The radial packing with aspect ratios 5.466 & 8.2 are producing high $\frac{K_e}{K_f}$ for all materials when compared with hollow packing arrangement.

	Brick	Steel	Iron	Aluminum
Radial Packing	3.433	5.25	5.65	6.7
Hollow Packing	3.58	5.02	5.225	5.9

Figure 6.16: Highest ETC comparison for radial and hollow packing with aspect ratio of 8.2

The aspect ratio of 5.466 with radial arrangement of aluminum spheres in a packed bed is producing highest $\frac{K_e}{K_f}$ of 7.52 due to the proper pressure drop and higher conduction near the walls as shown in Figure 6.15. Similarly, the aspect ratio of 2.733 with hollow arrangement of aluminum spheres in a packed bed is producing highest $\frac{K_e}{K_f}$ of 6.45 due to higher occupation of volume of spheres near bed wall as shown in Figure 6.14.

The steel, iron and aluminum packing spheres are producing about same ETC in radial packing and hollow packing arrangements for aspect ratios (Λ) 2.733 and 5.466. So, steel or iron spheres are used instead of aluminum spheres, which is less expensive. However, the radial packing with aspect ratio of 8.2 of aluminum spheres are producing higher ETC when compared to steel and iron. This is happening because of radial packing with smaller diameter of spheres shows more effect of conduction.

So, packing arrangement place crucial role on radial heat transfer. Although hollow packing arrangement of spheres produce less pressure drop compared to radial packing arrangement, but radial packing arrangement produce far better radial heat transfer.

59
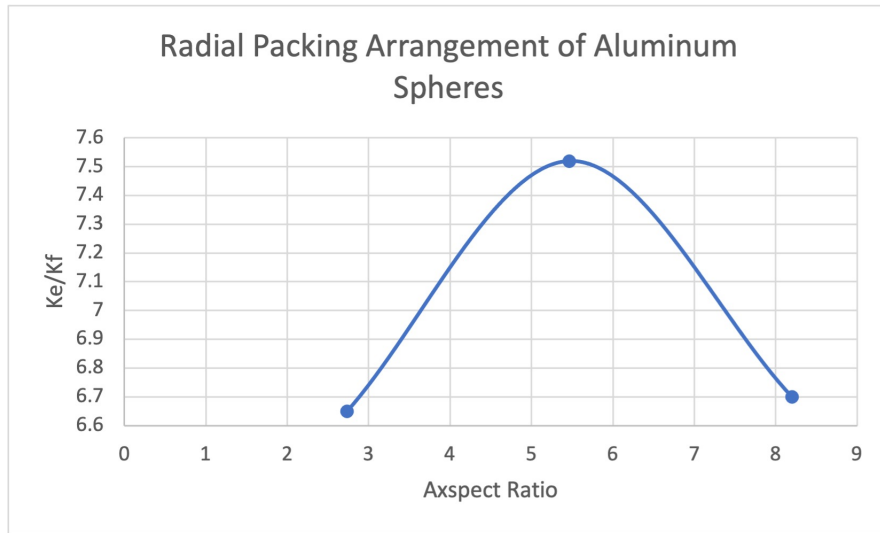
Figure 6.17: ETC comparison for radial packing of aluminum spheres with different aspect ratios
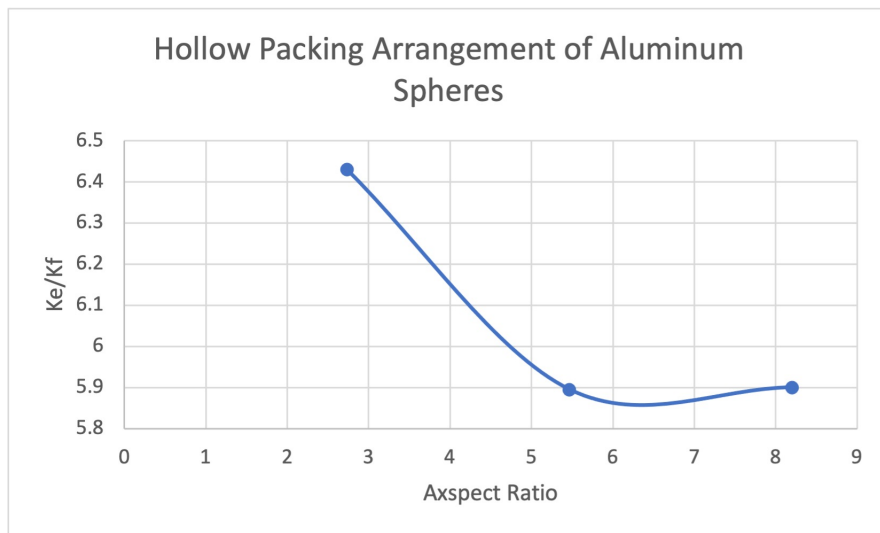
Figure 6.18: ETC comparison for hollow packing of aluminum spheres with different aspect ratios

The tread of ETC changes with respect to aspect ratio based on the packing arrangement. The Figure 6.17 shows that the ETC is rising is about 13%from aspect ratio of 2.733 to aspect ratio of 5.466. Then ETC is decreases is about 13%from aspect ratio of 5.46 to aspect ratio of 8.2. So, the aspect ratio of 5.466 is optimum for the radial packing arrangement from the results obtained to achieve better heat transfer.

The ETC is decreases as aspect ratio is increases in hollow packing arrangement as shown in Figure 6.18. The ETC decreases is about 8% from aspect ratio of 2.733 to aspect ratio of 5.466. Then ETC is about constant from aspect ratio of 5.46 to aspect ratio of 8.2. So, the ETC change is based on aspect ratio and packing arrangement.

Chapter 7

Conclusion and Future Work

7.1 Conclusion

The research presented in this thesis is a computational study of radial heat transfer performance in packed beds. Initially, 2D computational models are developed and simulated in COMSOL Multiphysics to see how porosity, aspect ratio, thermal conductivity of a packing material, packing arrangement, and Reynolds affect ETC. The aluminum packed circles with porosity of 0.316 produces highest $\frac{K_{eff}}{K_f}$ of 7.71 when compared to porosity 0.34, 0.387, and 0,505. Similarly, the brick particles of 0.505 produces lowest $\frac{K_{eff}}{K_f}$ of 4.109 produces lowest compared to other porosites. The regular packing of aluminum with aspect ratio 3.32 produces highest ETC of 7.71 and staggered packing of aluminum particles with aspect ratio 3.39 produces highest ETC of 14.34. So, the aluminum staggered packing circles with aspect ratio of 3.39 porosity of 0.316 produces better $\frac{K_{eff}}{K_f}$. There no affect of Reynolds number on radial heat transfer within laminar flow region. These 2D results provides an understanding that each and every parameter is important to see an affect of radial heat transfer in packed beds.

A 3D packed bed is designed to see the real affects of heater temperature, packing arrangement, aspect ratio, and thermal conductivity. The heater temperature shows an affect on ETC but not a considerable amount in both radial packing and hollow packing. The radial packing spheres of aluminum spheres with aspect ratio of 5.46 produces highest $\frac{K_{eff}}{K_f}$ of 7.52 and the radial packing of brick spheres with aspect ratio 5.46 produces lowest

$\frac{K_{eff}}{K_f}$ of 3.3. Similarly, The hollow packing spheres of aluminum spheres with aspect ratio of 2.77 produces highest $\frac{K_{eff}}{K_f}$ of 6.43 and the radial packing of brick spheres with aspect ratio 2.77 produce lowest $\frac{K_{eff}}{K_f}$ of 3.3. The steel and iron packing produce about the same $\frac{K_{eff}}{K_f}$ regardless of packing arrangement, aspect ratio and Reynolds number. The Reynolds number remains same for all cases within a laminar flow region.

7.2   Recommendations for Future Work

The different shapes such as cylindrical, raschig rings and irregular shapes of packing particles would use to see how packing particle shapes affects radial effective thermal conductivity.

This computational study also be done in transitional region ($10 < Re_P < 1000$) and see the affects of all other parameters and Reynolds number on ETC of a packed bed.

The experimental study could also be done for present study and compare with this study to see how accurately computational results are obtained.

Chapter 8

References

[1]Christie, J. Geankoplis., Transport Process and Unit Operations, PRENTICE HALL, Englewood cliffs, New Jersey, 1978.

[2]Warren, L. McCabe., Julian, C. Smith. and Peter, Harriott., Unit Operations of Chemical Engineering, McGraw-Hill Inc, New York, 1993.

[3]Demirel, Y., Sharma, R. N. and Al-Ali, H.H., "On the effective heat transfer in a packed bed", International journal of heat and mass transfer Journal, Vol. 43, (2000), pp. 327-332.

[4]Dixon, A.G., "Heat transfer in fixed beds at very low (Re_P <4) tube-to-particle diameter ratio", Ind. Eng. Chem. Res, Vol. 36, (1997), pp. 3053-3064.

[5]Freiwald, M.G. and Paterson, W.R., "Accuracy of model predictions and reliability of experimental data for heat transfer in packed beds", Chemical Engineering Science, Vol. 47, (1992), pp. 1545-1560.

[6]Smirno, E.I., Kuzmin, V.I. and Zolotarskii, I.A., "Radial Thermal Conductivity in Cylindrical Beds Packed by Shaped Particles", Chemical Engineering Research and Design, Vol. 82, (2004), pp. 293-296.

[7]Zehua, Guo., Zhongning, Sun., Nan, Zhang., Ming, Ding., Haozhi, Bian. and Zhaoming, Meng., "Computational study on fluid flow and heat transfer characteristic of hollow structured packed bed", Powder Technology, Vol. 344, (2019), pp. 463-474.

[8]Peng, Wenping., Xu, Min., Huai, Xiulan. and Liu, Zhigang., "CFD Study on Local Fluid-to-Wall Heat Transfer in Packed Beds and Field Synergy Analysis", Journal of Thermal science, Vol. 25, (2016), pp. 161-170.

[9]Borkink, J.G.H and Westerterp, K.R., "Influence of Tube and Particle Diameter on Heat Transport in Packed Beds", AIChE Journal, Vol. 38, (1992), No.5.

[10]Ying, Dong., Bahne, Sosna., Oliver, Korup., Frank, Rosowski. and Raimund, Horn., "Investigation of radial heat transfer in a fixed-bed reactor: CFD simulations and profile measurements", Chemical Engineering Journal, Vol. 317, (2017), pp. 204-214.

[11]Mariana, T. Zambon., Daniela, A. Asensio., Guillermo, F. Barreto. and German, D. Mazza., "Application of Computational Fluid Dynamics (CFD) for the Evaluation of Fluid Convective Radial Heat Transfer Parameters in Packed Beds", American Chemical Society, Vol. 53, (2014), pp. 19052-19061.

[12]Dong-Young, Lee., Myeong-Seon, Chae. and Bum-Jin, Chung., "Natural convective heat transfer of heated packed beds", International communications in heat and mass transfer Journal, Vol. 88, (2017), pp. 54-62.

[13]Yusuke, Asakuma., Itsuro, Honda. and Tsuyoshi, Yamamoto., "Numerical analysis of effective thermal conductivity with thermal conduction and radiation in packed beds", International journal of heat and mass transfer Journal, Vol. 114, (2017), pp. 402-406.

[14]Mandal, D., Sathiyamoorthy, D. and Vinjamur, M., "Experimental measurement of effective thermal conductivity of packed lithium-titanate pebble bed", Fusion Engineering and Design, Vol. 87, (2012), pp. 67-76.

[15]Lakshana Ravindranath, Huddar., "Heat Transfer in Pebble-Bed Nuclear Reactor Cores Cooled by Fluoride Salts," Ph.D. Thesis, UC Berkeley, 2016.

[16]Laszalo, Baranyi., Szilard, Szabo., Betti, Bollo. and Robert, Bordas., "Analysis of low Reynolds number flow around a heated circular cylinder", Journal of Mechanical Science and technology, Vol. 23, (2009), pp. 1829-1834.

[17]Wang, A.-B. and Travinicek, Z., "On the linear heat transfer correlation of heated cylinder in laminar crossflow using new representative temperature concept", International journal of heat and mass transfer Journal, Vol. 44, (2001), pp. 4635-4647.

[18]T. Atmakidis, E.Y.Kenig, and E.S. Kikkinides.,"CFD-based analysis of the wall effect on the pressuredrop in packed beds", European Congress of Chemical Engineering, Copenhagen, 2007.

[19]J. R. Sellers, M. Tribus, and J. S. Klein.,"Heat Transfer to Laminar Flow in a Round Tube or Flat Conduit—the Graetz Problem Extended", Transaction of ASME, Vol. 78, (1956), pp. 441-448.

[20]A. Haji-Sheikh., "Estimation of Average and Local Heat Transfer in Parallel Plates and Circular Ducts Filled With Porous Materials", ASME Journal of Heat Transfer, Vol. 126, (2004), pp. 400-409.

[21]Burmeister, L. C., "Convective Heat Transfer", Second Edition, John Wiley & Sons, Inc., New York, 1993.

[22]H. Nicolas, "Conjugate Heat Transfer", Comsol.com, Jan 2014.

[23]T. Atmakidis, and E.Y.Kenig.,"Numerical Investigations of Packed Bed Reactors with Irregular Particle Arrangement", 24th European Symposium on Computer Aided Process Engineering, Hungary, 2014.

[24]Tal Tsory,Nir Ben-Jacob, Tamir Brosh, and Avi Levy.,"Thermal DEM-CFD modeling and simulation of heat transfer through packed bed", Powder Technology, Vol. 244, (2013), pp. 52-60.

[25]Patil, S., Chintamani, S., Kumar, R., and Dennis, B. H., "Determination of orthotropic thermal conductivity in heat generating cylinder". ASME 2016 International Mechanical Engineering Congress and Exposition, American Society of Mechanical Engineer, pp-V011T15A016 doi:10.1115/IMECE2016-67918, 2016

[26]Patil, S., Chintamani, S., Grisham, J., Kumar, R., and Dennis, B., "Inverse Determination of Temperature Distribution in Partially Cooled Heat Generating Cylinder". ASME 2015 International Mechanical Engineering Congress and Exposition , pp -V08BT10A024-V08BT10A024, doi:10.1115/IMECE2015-52124,2015.

[27] Fabela, Oscar, Patil, S., Chintamani, S., and Dennis, B., "Estimation of effective thermal conductivity of porous Media utilizing inverse heat transfer analysis on cylindrical configuration". ASME 2017 International Mechanical Engineering Congress and Exposition,pp- V008T10A089-V008T10A089 doi:10.1115/IMECE2017-71559, 2017.

[28]Upreti R., Chintamani S., Patil S., Akbariyeh A, Dennis B., "Stochastic finite element thermal analysis of ball grid array package", Journal of Electronic packaging. doi: https://doi.org/10.1115/1.4050696, 2021.

[29]Sandeep Patil, Siddarth Chintamani, Brian H. Dennis, Ratan Kumar., "Real time prediction of internal temperature of heat generating bodies using neural network", Thermal Science and Engineering Progress, Volume 23, 2021, 100910, ISSN 2451-9049, https://doi.org/10.1016/j.tsep.2021.100910, 2021.